A Bio-Inspired Approach to Grab Design
Master Thesis

Michael Kunne

TUDelft
Delft
University of
Technology

Challenge the future
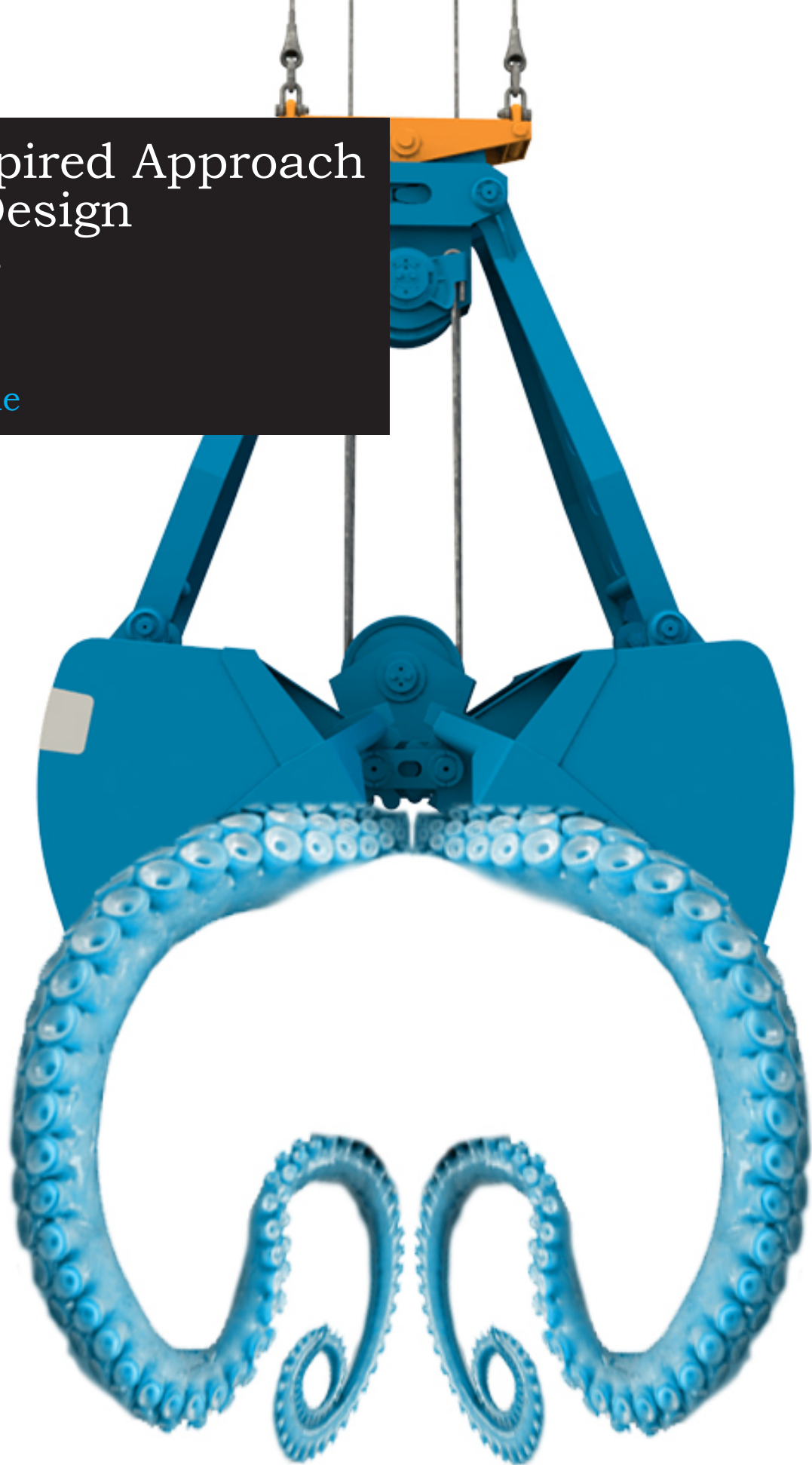
A Bio-Inspired Approach to Grab Design

Master Thesis

by

Michael Kunne

in partial fulfillment of the requirements for the degree of

Master of Science
in Mechanical Engineering

at the Delft University of Technology,

Student number:	4015215	
Supervisors:	Prof. dr. ir. P. Breedveld,	TU Delft
	Dr. ir. D.L. Schott,	TU Delft
	Ir. M. Scali,	TU Delft
	Ir. M. Corbeau,	Nemag B.V.
	Ir. G. van Koeveringe,	Nemag B.V.

TUDelft Delft University of Technology

Contents

A Bio-Inspired Approach to Grab Design

Michael Kunne

Abstract— **Grabs are efficient tools for bulk transhipment. However, there is always a need to increase grab efficiency. One way to increase grab efficiency is to reduce the weight of the grab, but lighter grabs tend to have insufficient penetration. In nature, organisms have found ways to penetrate a substrate without applying high forces to the substrate. The *Octopus kaurna* uses fluidization to burrow with ease. When a substrate fluidizes, its resistance to penetration reduces as it behaves fluid-like. In this work, fluidization is evaluated to use in a grab design and the effect of airflow, mass and depth are investigated. These parameters are varied using a penetration tool based on the current grab design and the effect on penetration trajectory is recorded. Increasing the mass of the penetration tool by 62.5%, 125%, and 187.5% increased the initial penetration with 59%, 109% and 150% for particles of $40-70\ \mu m$, and 55%, 88% and 138% for particles of $150-250\ \mu m$. The propagation velocity did not change significantly when the mass of the penetration tool was increased. Increasing the airflow with 100%, 200% and 300% increased the initial penetration with 230%, 777% and 646% for particles of $40-70\ \mu m$, and 85%, 112% and 143% for particles of $150-250\ \mu m$. The increasing depth of the penetration tool reduced the propagation velocity until a steady state depth was reached. These results are promising and show fluidization could be used to increase grab performance.**

I. INTRODUCTION

A. *General introduction on grabs*

Grabs have been designed for centuries. Probably one of the oldest grab designs is the scissor style grab designed by Da Vinci [1] (Figure 1). During the industrial revolution, the use of coal increased and due to poor road conditions, ships were used to transport coal over long distances. This increased the demand for grabs to unload ships effectively.
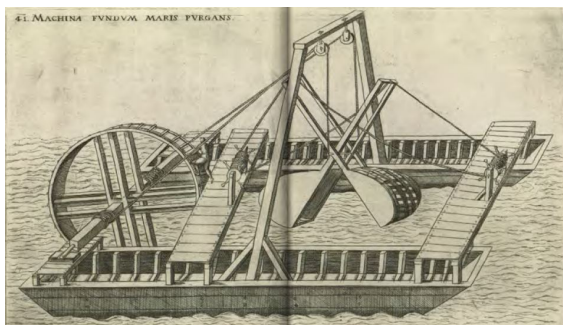
Fig. 1.   Primitive grab design by Leonardo Da Vinci [1].

A grab consists of a few key components (Figure 2). A grab can either be a two rope or a four rope grab. In both cases, half of the ropes are used for the lifting of the grab (hoisting ropes). The other half is used to operate the opening and closing of the grab (closing ropes). The closing force of the grab is amplified by using a pulley. The shells of the grab form a bucket which will hold the bulk material and the edge of the shell is the blade lip. The blade lip "cuts" through the material.
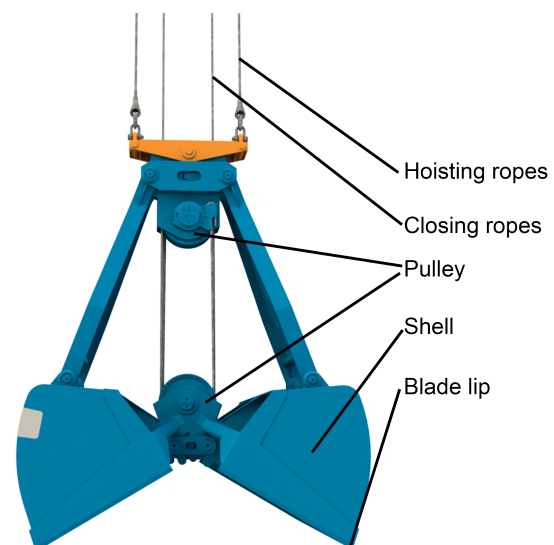
Fig. 2.   Basic parts of a four rope grab: hoisting ropes, closing ropes, pulley, shell and the blade lip. Image courtesy of NEMAG B.V. [2].

There are several Key Performance Indicators (KPI's) describing the performance of a grab. The KPI's of a grab are safety, mass, manufacturing costs, operational costs and average productivity [2]. The mass of a grab, especially with respect to the crane load capacity, is the key to the grab's efficiency. The mass of a grab can be over 40 tons, using 30-40% of the crane load capacity. The ratio between the mass of the grab and the crane load capacity should be as small as possible. This results in the maximum transfer of bulk material each cycle. Reducing manufacturing costs would improve the competitive position of the producer while the reduction of operational costs is a long-term benefit for both producer and client. The average productivity of a grab relies on the usage of the grab. Bulk transfer out of a ship consists of three stages: the free digging stage, the intermediate stage and the trimming/cleanup stage. Optimisation for one stage in particular or for the entire process can result in different designs.

B. *State of the art in grab technology*

The optimisation of the KPI's resulted in a variety of different grabs for different purposes and bulk materials (Figure 3). In this variety of designs, three main design
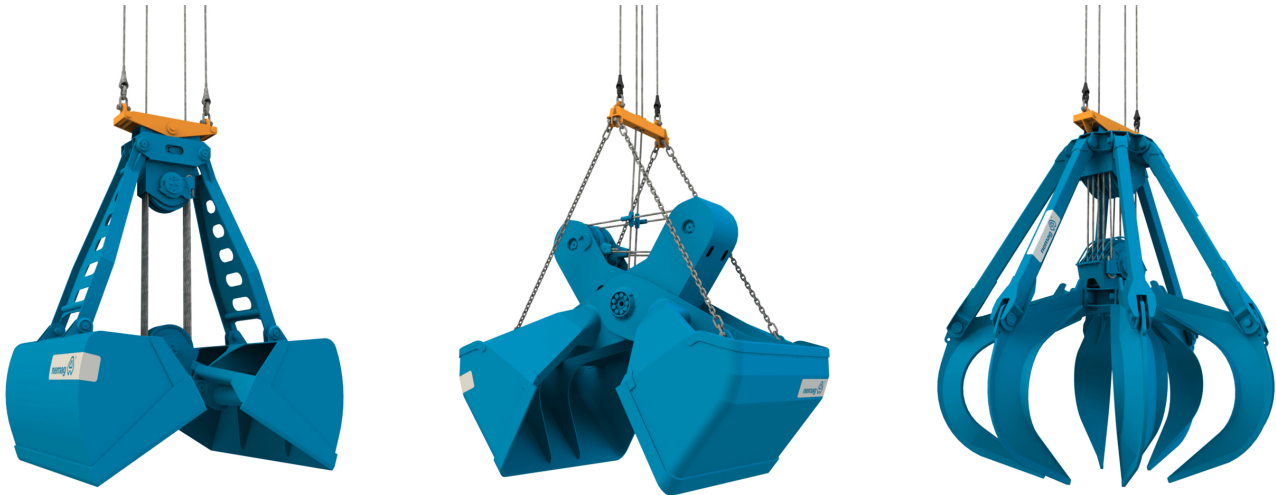
Fig. 3.   The three most used grab designs. From left to right, the Clam-shell, Scissor and the Cactus/Orange peel grab. Image courtesy by NEMAG B.V. [3].
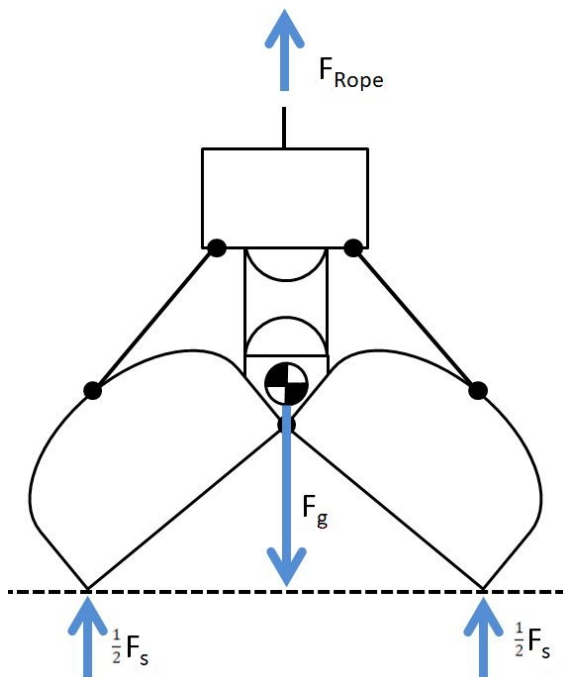
Fig. 4.   Forces acting on a grab while closing (simplified grab model). F_{Rope} is the force in the closing ropes. F_s is the reaction force of the substrate on the blade lips. F_g is the gravitational force due to gravity acting on the centre of mass.

directions can be distinguished: the Clam-shell grab, the Scissor grab and the Cactus/Orange peel grab.

The most common grab is the Clam-shell grab. The Clam-shell grab can handle most types of bulk material including coal, ore, minerals, biomass, fertiliser, etc. The Clam-shell grab consists of two shells that are closed by a pulley system that increases the closing force. By increasing the number of pulleys, the closing force of the grab can be trimmed to fit the

bulk material requirements. Due to the simple design of the Clam-shell grab, it is lightweight and it is optimised for its high productivity in the free digging stage. The Clam-shell grab has a deep and circular digging pattern. This digging pattern is sub-optimal for the trimming/cleanup stage as it cannot collect material over a large horizontal surface.

To obtain a higher average productivity throughout all the stages of emptying a ship, the Scissor grab was designed. The Scissor grab can handle most types of bulk, like coal, ore, minerals, biomass, etc. It consists of two shells connected to two long arms. The arms are connected to each other in their centre, and a single pulley system connects the two arms at their extremities. This configuration results in a more horizontal digging pattern and a wider spread of the grab. This property is especially beneficial in the trimming/cleanup stage of emptying a ship, resulting in the Scissor grab's high average productivity. Another feature of this design is its relatively constant closing force throughout its closing trajectory.

The Cactus/Orange peel grab has an entirely different design. Its main purpose is the transhipment of scrap metal, biomass and animal feed. It consists of multiple arms in a circular configuration. The force transmission of the closing ropes goes through a central pulley configuration increasing the closing force with each additional pulley similar to the Clam-shell grab.

Current research focuses on the optimisation of the current grab designs and on finding new hybrid designs. For the optimisation of current grabs, Discrete Element Models (DEM) for grab simulation have been created [6]. These models can give information about the effects of varying grab parameters like width, mass and shell shape without building a prototype.

C. Problem definition

A grab has many advantages as a means to empty a ship. It is very simple in production, usage and maintenance. The

most important downside of the grab is its mass, which can be over 40 tons. This can take up to 40% of the crane load capacity. This means that only 60% of the crane safe working load can be used for the transhipment of bulk. The essence of the problem is that the grab cannot simply be made lighter without consequences for its digging capabilities. The work of Lommen [6] shows that a heavy grab has good digging capabilities, but that it takes a large share of the crane safe workload. Due to the high mass of the grab, the amount of material that can be transferred each cycle is low. The decrease in transferred material per cycle reduces the grab efficiency. A light grab increases the amount of bulk that can be transported each cycle. However, its low mass prevents the grab from penetrating into the substrate and filling its shells completely, resulting in a net loss of efficiency. Analysing the effect of mass on the efficiency of grabs, shows that there is an optimum mass to achieve the maximum performance in current grabs. When we analyse the forces acting on a grab at the moment of closing, we can see that the mechanism that closes a grab increases the problem of insufficient penetration. Figure 4 shows the forces acting on a grab at the moment of closing. As the ropes can only pull on the grab, there is an upward force reducing the pressure on the blade lips. The combination of the mass requirement and the upward force causes an optimisation problem that cannot be solved by using the conventional grab design.

D. *Aim of the study*

The aim of this work is to find and evaluate a new digging mechanism for the use in a grab, using a bio-inspired approach. The new digging mechanism is evaluated in order to make weight reduction possible, while maintaining the digging properties of the grab.

E. *Layout of the report*

In Section II, the principle of fluidization is explained. The basic theory is explained, and examples of the application of fluidization in industrial applications are given. Section

II concludes by giving outlines on how fluidization can be used in a grab. Section III discusses the experimental design, declaring the independent and dependent variables and showing the experimental set-ups used for the experiments. Section IV shows the procedure followed during the first two experiments and shows the results. Section V describes the procedure and the results of the third experiment. The results of the experiments are interpreted in the discussion in Section VII. The discussion also covers the limitations of this work and gives recommendations concerning future work. This paper ends with a conclusion in Section VIII.

II. FLUIDIZATION

A. *The biological mechanism of fluidization*

Organisms in nature can use many methods to burrow. When looking at these methods, they can be categorised as compaction [7], excavation [8], fluidization [8][7][9][10] and breaking down [8][11]. Not all burrowing principles are interesting to evaluate for the application in grabs. In order to be promising, a principle has to be scaleable to the size of a grab, able to perform in a time interval of several seconds and keep the substrate intact. Fluidization fulfils these requirements, as it does not suffer from scaling limitations like compaction and excavation and can be much faster than breaking down. Fluidization is a mechanism used by organisms like the sandfish [12][10], sand-snake [12], several bivalves [13][14], and the *Octopus kaurna* [5].

During fluidization, the properties of a granular material changes and the material behaves like a fluid. In this work, we will focus on the *Octopus kaurna*, also known as the Southern Sand Octopus. Even though its burrowing mechanism seems simple, it is fast. The burrowing rate index calculates the ratio between the burrowing rate of an animal and its mass (Equation 1).

$$BRI = \frac{\sqrt[3]{m}}{t} \cdot 100 \qquad (1)$$

Where the burrowing rate index (BRI) is expressed in terms of the animal mass m in [g] and the burrowing time t
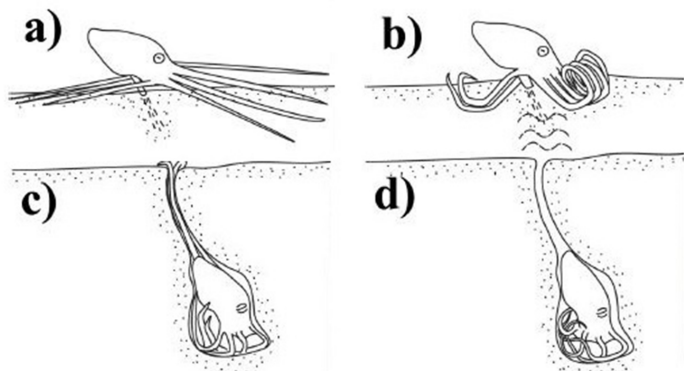
Fig. 5.   The burrowing cycle of the *Octopus kaurna* [4]. a) The *Octopus kaurna* uses its mantle and syphon to fluidize the sediment below it. b) The sediment fluidizes and the *Octopus kaurna* moves its arms into the sediment. c) At full fluidization of the sediment, the *Octopus kaurna* pulls itself deep into the sediment. d) The Octopus removes his arms to form a chimney and clears the chimney from loose sand. Adapted from Montana et al (2015) [5].

in [s]. With a burrowing rate index of 14.89 in fine-medium substrates, the *Octopus kaurna* is considered very fast (a burrowing rate index above 2 is considered rapid burrowing) [5][15]. The *Octopus kaurna* lives in the ocean to the south of Australia [4]. It can reach a span up to 50 *cm*. As it cannot change colours like many other octopuses, it needs another way of hiding from predators. The *Octopus kaurna* hovers above the sediment and starts to use its mantle and syphon to fluidize the sediment below it. When the sediment starts to fluidize, the *Octopus kaurna* moves its arms into the fluidized sediment. At full fluidization of the sediment, the *Octopus kaurna* pulls itself deep into the sediment and makes a chimney with two of its arms. The octopus removes his two arms from the chimney and, with strong exhales, it clears the chimney from loose sand (Figure 5).

B. *Basic theory of fluidization*

Most theories in the field of fluidization consider an upward airflow [16][17]. These theories are used to understand the behaviour of a granular material under the influence of fluidization. A granular material behaves like a solid in static conditions because of the formation of stress chains between particles (Figure 6a). The weight of every individual particle adds to the increase in friction between the next particles in the chain. As a result, the friction between particles scales with depth and moving particles becomes harder. There are a few different ways to avoid the increase of friction with depth. If the stress chains are interrupted, the friction between particles is eliminated, and the particles can move freely. This phenomenon is called 'fluidiziation'. The first method to achieve fluidization of a substrate is vibration. When the particles get excited, there will be short intervals at which

the stress chains are interrupted. During this short amount of time, a particle can be displaced. The second method, is to inject a fluid in the substrate (Figure 6b). In this type of fluidization, a balance of forces is reached between gravity forces and the resistance caused by the moving fluid (Figure 7). There are multiple methods for estimating the minimum fluidization velocity, the fluid velocity at which fluidization first occurs. The most popular method to estimate the minimum fluidization velocity is based on the work of Wen and Yu [18][16]. First, the Archimedes number Ar, which is the ratio between external forces and internal viscous forces, is calculated with the following equation:

$$Ar = \frac{\rho_g d_p^3 \left(\rho_p - \rho_g\right) g}{\mu^2} \qquad (2)$$

where ρ_g is the gas density, ρ_p is the particle density, d_p is the diameter of the particles, g is the gravity and μ is the fluid viscosity. The Archimedes number can then be used to calculate the Reynolds number at the minimum fluidization velocity ($Re_{p,mf}$) by solving the following equation:

$$Ar = 1,650 Re_{p,mf} + 24.5 Re_{p,mf}^2 \qquad (3)$$

Using this Reynolds number the minimum fluidization velocity u_{mf} can be calculated using:

$$Re_{p,mf} = \frac{\rho_g u_{mf} d_p}{\mu} \qquad (4)$$

From equations 2, 3, and 4 it can be observed that the density of the particles and the density of the fluid, the particle size and the fluid viscosity are of importance.

a)   b)
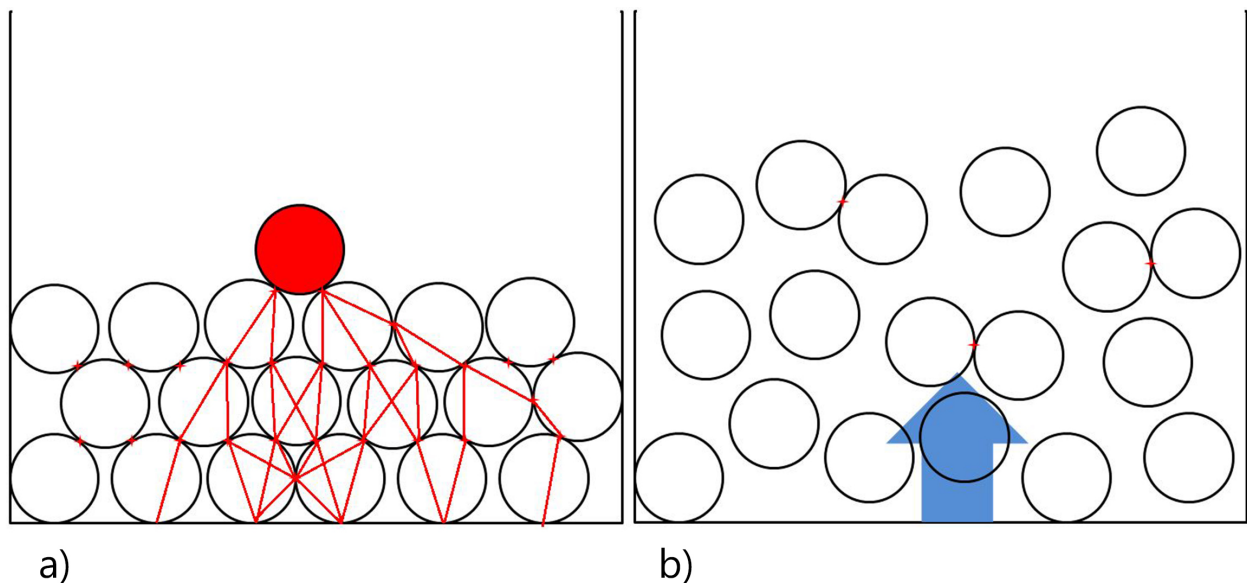
Fig. 6.   a) The concept of stress chains. The circles represent particles, and the red lines represent the uninterrupted stress chains originating from the top red particle. Every layer adds weight to the previous one, thus increasing the internal friction as a function of depth. Contact points between particles are indicated by red crosses. b) Interruption of stress chains during fluidization. Circles represent particles. The blue arrow shows the flow direction. Red crosses indicate contact between particles.

Aside from the density of the particles and the density of the fluid, the particle size and the fluid viscosity, the permeability of a substrate is another factor in fluid-particle interaction. The permeability is a measure of how easy a fluid can pass through a substrate. When considering a hydraulic pressure i and a permeability coefficient k, equation 5 calculates the apparent fluid velocity V [19].

$$V = ki \tag{5}$$

where k can be estimated using Hazen's equation:

$$k = CD_0^2 \tag{6}$$

where C is a constant based on the substrate, for sand like materials in the order of 10^{-2} and D_0^2 is the substrate effective particle size.
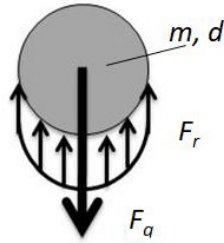
Fig. 7. Balance of forces during fluidization. When a particle with a mass m and diameter d is fluidized, the gravitational force F_g and the fluid friction F_r are equal.

C. Effective viscosity models

When a substrate is fluidized, it can be modelled as a fluid. Instead of viscosity used in fluids, for granular substrates, the effective viscosity is used. The effective viscosity is used to express the resistance to shear stress of a granular material as if it was a fluid. In a granular medium, the effective viscosity is dependent on the void fraction of the substrate and the viscosity of the fluid in between the grains. The void fraction is the fractional amount of the volume of a granular material that is not filled with particles of the material. The void can be filled with, for example, air or water. The void fraction has to be experimentally determined for a substrate with unequal particle sizes and depends also on the treatment (e.g. vibration and compaction).

A way to change the effective viscosity of a granular substrate is to change the void fraction. The following models describe the effective viscosity of a granular medium as a function of the void fraction.

Frankel and Acrivos [20].

$$\mu_{eff} = \mu_f \left(1 - \left(\frac{1-\phi}{1-\phi'}\right)\right)^{-2.5\phi'} \tag{7}$$

Krieger and Dougherty [21].

$$\mu_{eff} = \mu_f \left(\frac{9}{8}\right) \frac{\left(\frac{1-\phi}{1-\phi'}\right)^{\frac{1}{3}}}{1 - \left(\frac{1-\phi}{1-\phi'}\right)^{\frac{1}{3}}} \tag{8}$$

Eilers, Ferrini et al [22][23].

$$\mu_{eff} = \mu_f \left[1 + \left(\frac{1.25(1-\phi)}{1 - \frac{1-\phi}{1-\phi'}}\right)\right]^2 \tag{9}$$

Maron and Pierce [24].

$$\mu_{eff} = \mu_f \left(1 - \frac{1-\phi}{1-\phi'}\right)^{-2} \tag{10}$$

Where the effective viscosity μ_{eff} is a function of the pore fluid viscosity μ_f and the void fraction ϕ. ϕ' is the minimum void fraction of the substrate, it has to be experimentally determined for irregularly shaped substrates. The models all show roughly the same behaviour, but they are all made to fit experimental data, especially in the low void fraction region the models differ significantly as shown in Figure 8. The relative viscosity approaches infinity at a low void fraction, meaning the substrate behaves like a solid. At higher void fractions the effective viscosity quickly drops and approaches the viscosity of the pore fluid as the void fraction goes to 1.
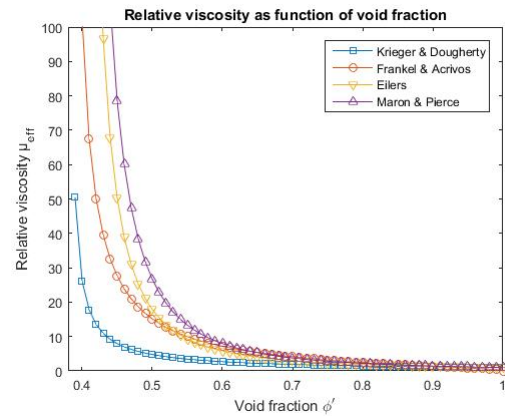
Fig. 8. Models based on random packing of spheres with an undisturbed void fraction of 0.38 and increasing to a void fraction of 1 [25].

D. The Geldart classification of particles

When considering spherical particles, the fluidization properties of a substrate can be estimated by the Geldart classification (Figure 9). The classification has four categories: Class A, B, C, and D. The classes are based on the particle size and difference in density between the substrate and the fluid [26]. Class A and Class B particles are easiest to fluidize. The particles are big enough that cohesion forces are not dominant nor are they too large for aerodynamic forces to suspend the particles. Class A particles are easiest to fluidize and show a clear transition between minimum fluidization velocity and bubble formation. Class B particles

are still fluidized at low fluid velocities, but bubbles are formed at the minimum fluidization velocity. The smallest particles, Class C, are so small that cohesion forces become the dominant force. Cohesion forces make the particles stick together, and fluidization in a static environment becomes hard. In Class D particles the gravitational forces are hard to overcome by the aerodynamic forces. High fluid velocities are needed for fluidization and sprouting occurs. Sprouting is the formation of channels with high fluid velocity where particles will move up. Outside of these channels the particles move down. Fluidization of Class C and Class D particles can be improved when using additional measures like stirring [27] or rotational flow [28][29].

E. Industrial applications of fluidization

Using fluidization in industrial applications is not entirely new. A patent search was conducted to see if and how fluidization is already applied in grabs or other industries. In chemical plants it is used for fluidized bed reactors [30], in dredging it is used to loosen the marine sediments [31][32][33], and it is used to transport granular materials [34].

In a fluidized bed reactor, a fluid is injected from the bottom of a reactor. In this application fluidization aids in the heat and mass transfer inside the reactor, reducing process times [35]. In dredging applications, jets of pressurised water and air are injected into marine sediments to loosen them and ease their removal [32][33]. In the field of the transportation of granular materials, one patent uses fluidization from above as a method to loosen and remove soil. A.C. Brigs and R.D. Nathebson [34] describe the use of rotating supersonic air-jets and a vacuum for the removal of soil. The field of bulk transhipment, however, does not yet use fluidization to enhance grab performance.

F. Fluidization applied to a grab

The principle of fluidization cannot be applied to a grab for bulk transhipment without any adaptations. One important difference between fluidization in nature and bulk transhipment is the substrate. In the fluidization example in Section II-A the substrate is saturated with water. In bulk transhipment, most substrates have to be completely dry. In order to keep the substrate dry, water can not be used as a fluid in the fluidization process. When taking availability and compatibility into consideration, using air as a fluidizing fluid remains the only feasible option. According to the theory in Section II-D the difference in density between water and air makes fluidization more challenging as higher fluid velocities are needed.

A difference with existing applications of fluidization is the method of fluidization used. Due to the size of a cargo hold, it would be energy consuming to fluidize the entire bulk of the substrate. To avoid this, the *Octopus kaurna* is used as inspiration. We can fluidize from above the substrate to achieve local fluidization (Figure 10). To make fluidization from above possible, the current blade lip design is adapted. This design is used as the penetration

tool for the experiments. The dimensions of the penetration tool are $68\ mm * 40\ mm * 150\ mm$. A system of air chambers is incorporated into the design to distribute the airflow evenly to the tip of the blade lip (Figure 11). At the tip of the penetration tool there is a nozzle consisting of an opening of $1\ mm$ width and a length of $65\ mm$. Another change to the design is the symmetry of the blade lip. In current applications the blade lip is asymmetric but to avoid uneven horizontal forces during the experiments, described in Section IV and Section V, a symmetrical design is used.

III. Experimental design

A. Goal of the experiments

The theory in Section II-B, describes the main parameters that influence fluidization: the substrate properties, fluid properties, and depth. For the current grab design, mass is an important parameter. To evaluate the influence of these parameters, a series of three experiments is designed.

The goal of the first experiment is to evaluate the influence of the mass of the penetration tool on the penetration trajectory. The penetration trajectory is defined as the penetration depth as a function of time. The second experiment is designed to evaluate the influence of airflow on the penetration trajectory. The first two experiments also evaluate the difference between two types of substrate, specified in Section III-D. The third experiment is designed to evaluate the influence of depth on the penetration trajectory.

B. Independent and dependent variables

In Experiment 1 the mass of the penetration tool and the substrate are the independent variables. For Experiment 2 the airflow and the substrate are the independent variables. In Experiment 3 airflow is the independent variable. The measured dependent variable for all three experiments is the penetration trajectory.

C. Hypotheses

For Experiment 1, two hypotheses are formulated:

- An increase in penetration tool mass, increases the initial penetration.
- An increase in penetration tool mass, increases the propagation velocity.

According to the theory, the friction between particles scales with depth. When the mass of the penetration tool increases, it will be able to overcome these forces thus increasing the initial penetration. A higher mass of the penetration tool will result in a higher gravitational force F_g. As the tool does not change in dimension, it will be able to overcome shear resistance caused by the fluidized substrate more easily, resulting in a higher propagation velocity.

For Experiment 2, two hypotheses are formulated:

- An increase in airflow, increases the initial penetration.
- An increase in airflow, increases the propagation velocity.

The increase in airflow will cause a higher air velocity at the tip of the penetration tool. This will blow substrate
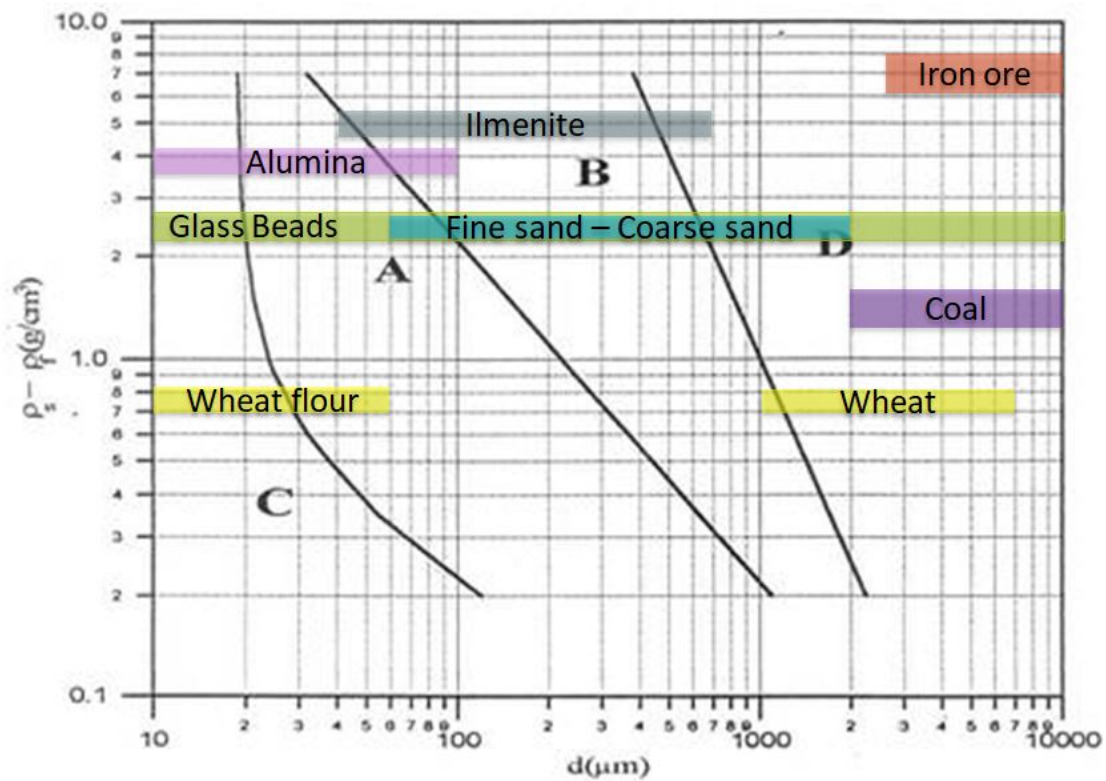
Fig. 9. The Geldart classification of particles and some encountered ranges of bulk materials. On the X-axis the diameter of the particles d is shown in $[\mu m]$ and on the Y-axis the density difference between the fluid and the particles $(\rho_s - \rho_f)$ in $[g/cm^3]$ is shown. A, B, C, and D represent the different regions in the graph where particles have a specific fluidization behaviour. Adapted from Geldart (1973) [26].
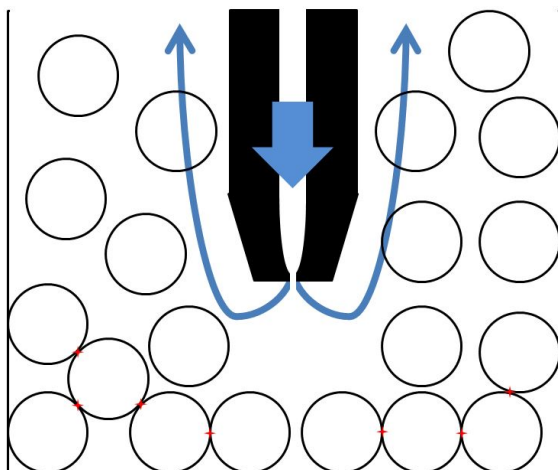
Fig. 10. Local fluidization around penetration tool. Circles represent the particles. Blue arrows show the airflow direction. Red crosses indicate the contact between particles. Close to the penetration tool (black) the particles are fluidized and there is little contact between particles. Further away from the tool, particles are not fluidized and there are more points of contact between particles.

aside and increase the void fraction. As explained in Section II-C, an increase in void fraction will result in a decrease of effective viscosity. The local drop in effective viscosity will reduce the resistance against penetration resulting in a higher initial penetration and propagation velocity.

For Experiment 3, two hypotheses are formulated:

- An increase in penetration depth, reduces the propagation velocity.
- An increase in airflow, increases the initial penetration.

According to the theory of stress chains, the friction between particles will increase with depth. Breaking these chains will, therefore, be increasingly difficult. This increase in difficulty will result in a lower rate at which the stress chains are broken and therefore the propagation velocity will reduce as the depth increases. The second hypothesis is a continuation of Experiment 2 and follows the same reasoning as stated before (Section IV-B).

D. Substrate selection

In agreement with the theory in Section II-D, the particles that are used should be either in Class A or B. These particles are the easiest to fluidize, as the particles in these classes have low mass and the cohesion force is not dominant. The most common particles encountered in bulk transport are placed in the Geldart classification (Figure 9). The density of air is less than 1% of these materials and is therefore neglected. As shown, there are bulk materials that are classified as class A or B according to the Geldart classification, namely: sand, ilmenite, and alumina. Glass beads are added to this graph although it is not considered a
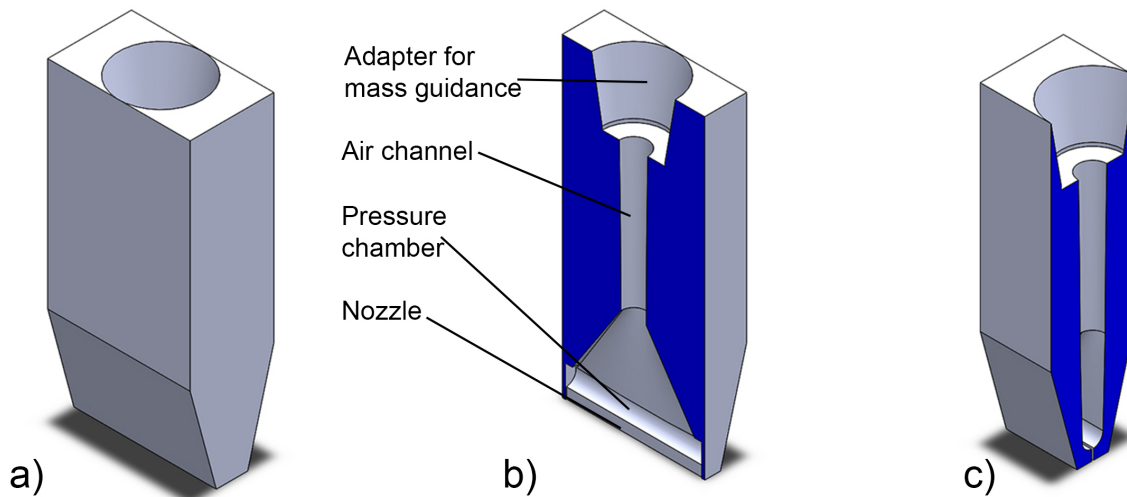
Fig. 11.   a) The symmetric model of the blade lip that is used as penetration tool. b) Section view of the internal components of the penetration tool. The adaptor for mass guidance makes it possible to add additional mass to the penetration tool. The air channel guides the airflow to the pressure chamber. The nozzle injects the air into the substrate. c) Section view perpendicular to the section view of b).
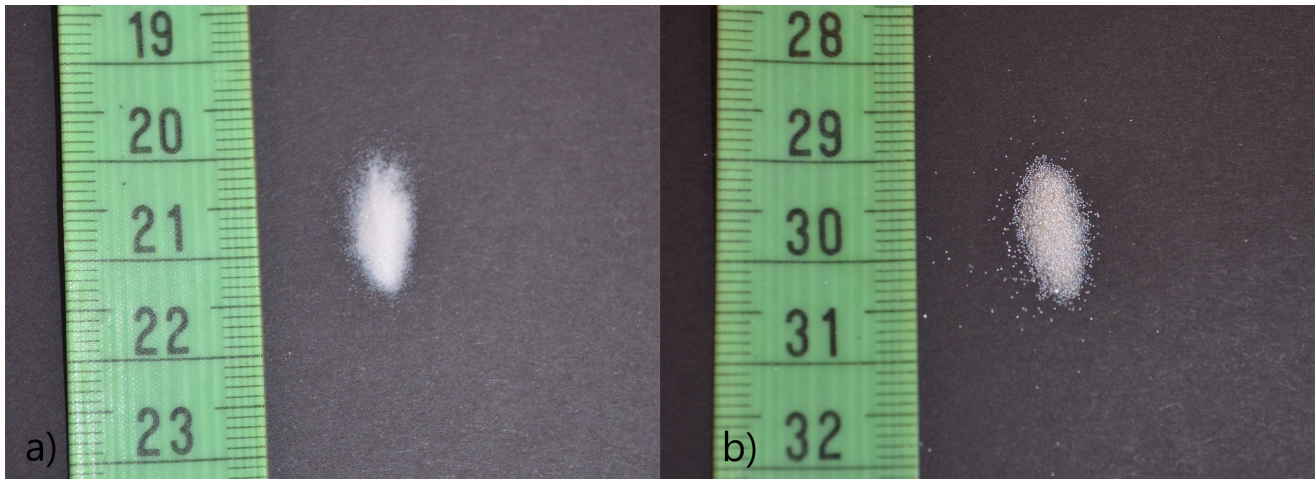
Fig. 12.   Glass beads used in the experiments with a diameter of a) $40 - 70 \; \mu m$ and b) $150 - 250 \; \mu m$.

bulk material. Glass beads are often used to substitute bulk material in experimental settings. The consistency in size and shape makes glass beads an excellent testing material and it is available in almost every size. Because of these properties, glass beads are used for the experiments in this work. Two sizes of glass beads are used to represent the A and B class. The glass beads in Class A have a size range between $40 - 70 \; \mu m$ diameter. The glass beads in Class B have a diameter between $150 - 250 \; \mu m$ (Figure 12). The density of glass beads is $2.5 \; g/cm^3$. Using equation 2, 3, and 4, the minimum fluidization for these glass beads can be estimated. Using the properties of air at a temperature of $300 \; K$ [36], the minimum fluidization velocity equals $0.0013 \; m/s - 0.0039 \; m/s$ for Class A glass beads and $0.0181 \; m/s - 0.0497 \; m/s$ for Class B glass beads. However, these velocities are valid for an uniform and upward airflow. In the case of local air injection from above, the airflow will

not be uniform. As the distribution of the air through the glass beads is unknown, calculation of local air velocities is not possible and the airflow for the experiments have to be determined with a trial.

E. Experimental set-up for Experiment 1 and 2

To test the effects of different parameters on the fluidization, an experimental set-up was designed (Figure 13). The set-up has to be able to:

- Receive pressurised air from a source.
- Control and measure the airflow and air pressure.
- Vary the mass of the penetration tool.
- Measure and record the penetration trajectory as a function of time.

First, an enclosure was built to contain the substrate and to guide the penetration tool. The dimensions of the enclosure are $500 \; mm * 700 \; mm * 70 \; mm$ (height $*$ width $*$ depth).
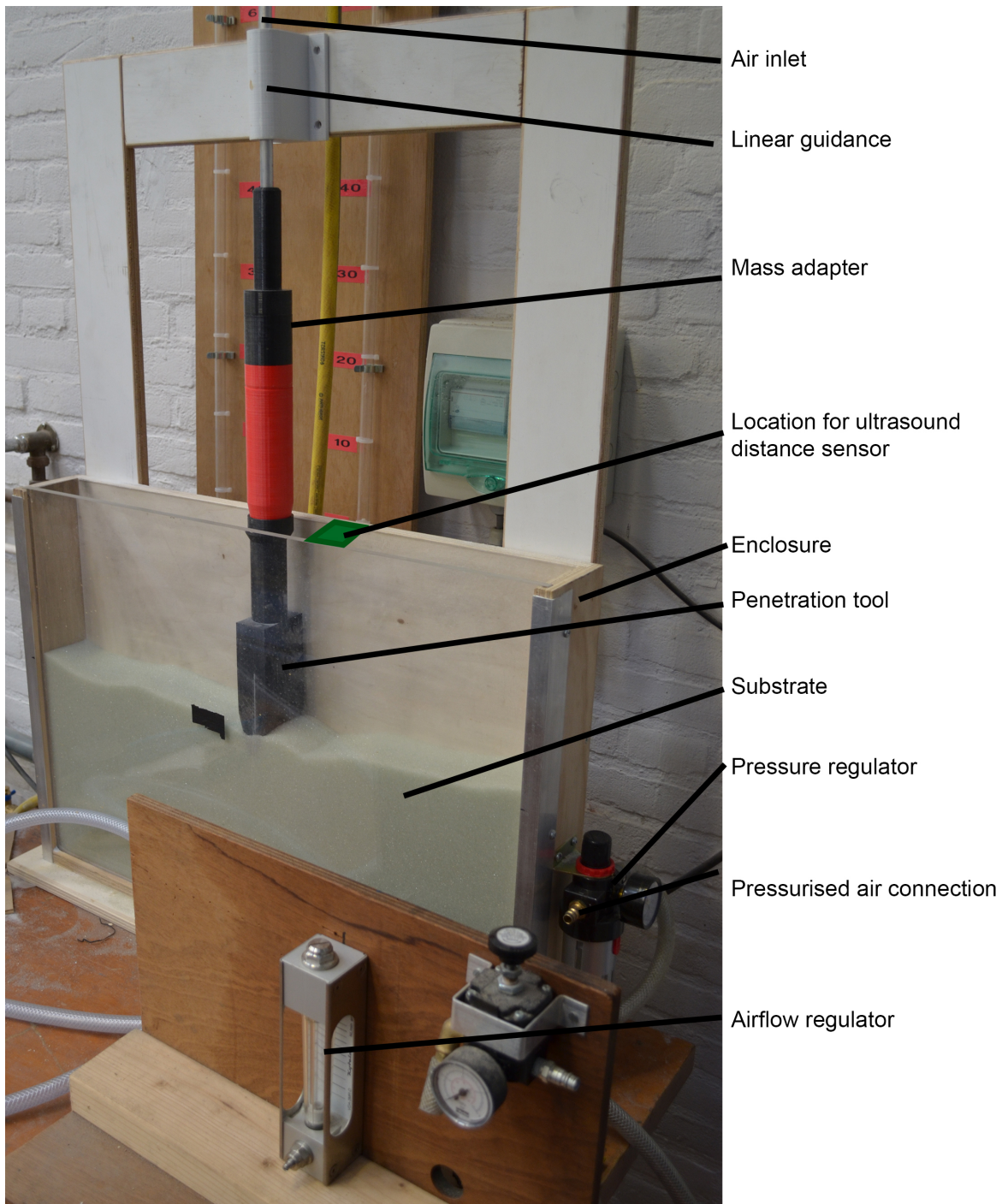
Fig. 13. Experimental set-up of Experiment 1 and 2. At the top there is a tube to guide the airflow to the penetration tool. A linear guide restricts horizontal movement of the penetration tool. The mass adaptor makes it possible to add weights to the penetration tool. The enclosure contains the substrate. The pressure regulator, pressurised air connection, and airflow regulator control the airflow supplied to the penetration tool.
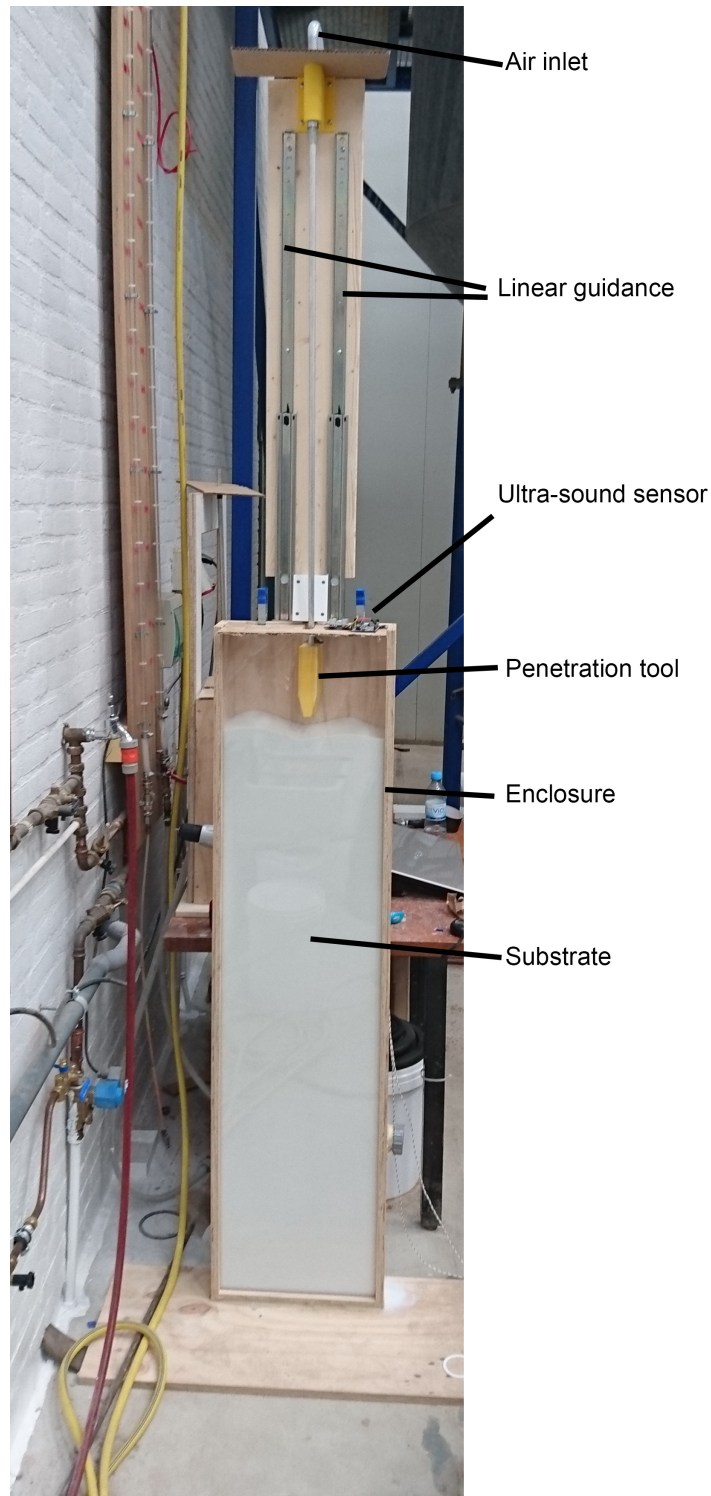
Fig. 14.   Experimental set-up of Experiment 3. The air inlet is situated on top of the set-up and a aluminium tube connects it to the penetration tool. Two linear guides enforce vertical movement. The ultrasound distance sensor is placed on top of the enclosure.

The enclosure was built of plywood. To increase the amount of visual information that could be obtained, one side of the enclosure was made of transparent Plexiglas. To keep possible wall effects equal at both the front and back surface of the enclosure, a thin Plexiglas plate was placed on the backside as well.

For the airflow three components were used: a pressurised air supply, a pressure controller, and a flow controller. The supply of pressurised air was taken from a central distribution network. The pressure of the central distribution network can vary between 6 bar and 7 bar. To ensure constant pressure during the experiments the Silverline "Air Line Filter Regulator" was used. The Silverline "Air Line Filter Regulator" has a pressure range between 0.5 bar and 8.0 bar. To control and measure the airflow the VDA-3MR-D "In Line Floating Ball Flow Meter" was used with a range of $0 - 300$ l/min and an accuracy of 5% [37]. Furthermore the "In Line Floating Ball Flow Meter" needed to be set manually, adding a human error of approximately 5 l/min.

The penetration depth was measured using the HC-SR04 ultrasound distance sensor. The ultrasound distance sensor has a accuracy of 3 mm over its range of 20 mm - 4000 mm [38].

To alter the mass of the penetration tool in Experiment 1, gym weights were used. These weights can be stacked on the penetration tool and have a mass of 0.5 kg and 1.0 kg. A 3D printed interface with a conical connection ensured that the weights were aligned with the centre of the tool.

F. *Experimental set-up for Experiment 3*

The experimental set-up used for Experiment 3 is mostly the same as for Experiment 1 and 2. The same supply and control systems for the airflow were used. Additionally, the same ultrasound distance sensor was used. The enclosure differs in dimensions and measures 1500 $mm * 350$ $mm * 70$ mm (Figure 14). The width of the enclosure was reduced to limit the amount of glass beads that needed to be used, and observations of the first two experiments suggested this could be done without affecting the outcome of the experiments. Similar to the first enclosure, both front and backside of the enclosure have a Plexiglas surface. The enclosure was filled to a height of 1200 mm with glass beads. It was not possible to use the same sliding bearing as for the first set-up due to the increased travel of this set-up. Using the sliding bearing creates too much play. To solve this, a set of drawer slides was used to guide the penetration tool vertically. Working with glass beads of Class A caused dust formation in the first two experiments, especially at a higher airflow. For Experiment 3, the linear guidance system would degrade fast while working in a environment with airborne glass beads. Therefore we decided to perform this experiment only with particles of Class B ($150 - 250$ μm).

IV. EXPERIMENTAL EVALUATION: THE EFFECTS OF MASS AND AIRFLOW

A. *Data acquisition and analysis*

To measure the penetration trajectory, an ultrasound sensor was installed at the top of the enclosure. The ultrasound sensor was connected to an Arduino Uno which supplied the power, controlled the measurement frequency and sent the measured data to a computer system. The distance data from the ultrasound sensor is sent to a computer over a serial connection. The serial monitor of the Arduino software displayed the incoming data and these data were copied to separate excel files for each repetition. Because of dust formation during the experiments, the data had some noise that had to be filtered out. Removal of the noise was done using the smooth function in Matlab (version: 2015b). The rest of the analysis was also performed in Matlab. (for the Matlab code used in Experiment 1 and 2, see Appendix B and for the code used to program Arduino Uno, see Appendix C). The connection scheme of the Arduino Uno is shown in Figure 16. To analyse the significance of the results a one-way ANOVA was used and their p-values are given.

Figure 15 shows the definition of terms used to describe the data obtained from the experiments. The first part of the penetration trajectory is called the initial penetration. The initial penetration happens in the first second after the tool is released and can be compared to the reference data, as the reference data only has an initial penetration. After this first second the penetration tool keeps propagating through the substrate. The second part of the penetration trajectory can be described in terms of propagation velocity. The propagation velocity was calculated as the average velocity between 10% and 90% of the experiment. The reference data used the same mass as the other data, but the repetition was performed without airflow. The reference data aids the comparison between the fluidization assisted penetration and conventional penetration.

B. *Procedure*

1) Experiment 1: variation of penetration tool mass: For the first experiment, the airflow was held at a constant level of 25 l/min while we varied the mass of the penetration tool. 25 l/min Was selected based on a pilot experiment showing a low airflow would give the clearest results. The experiment was conducted on both substrates. 0.8 kg Was the minimum mass used because it is the weight of the set-up itself. 0.5 kg Was added for each subsequent experiment, and every configuration was repeated six times. Table I lists the experimental conditions. The order of testing was randomised for the mass of the penetration tool.

At the start of each trial, the substrate was levelled. The mass of the penetration tool was adjusted to either 0.8 kg, 1.3 kg, 1.8 kg, or 2.3 kg to the tool. The PVC tubing retained some pressurised air, resulting in a small burst of air when the valve is opened. To reduce the disturbance of this burst of air on the substrate, the airflow was initiated at a height relative to the surface of 200 mm. When the
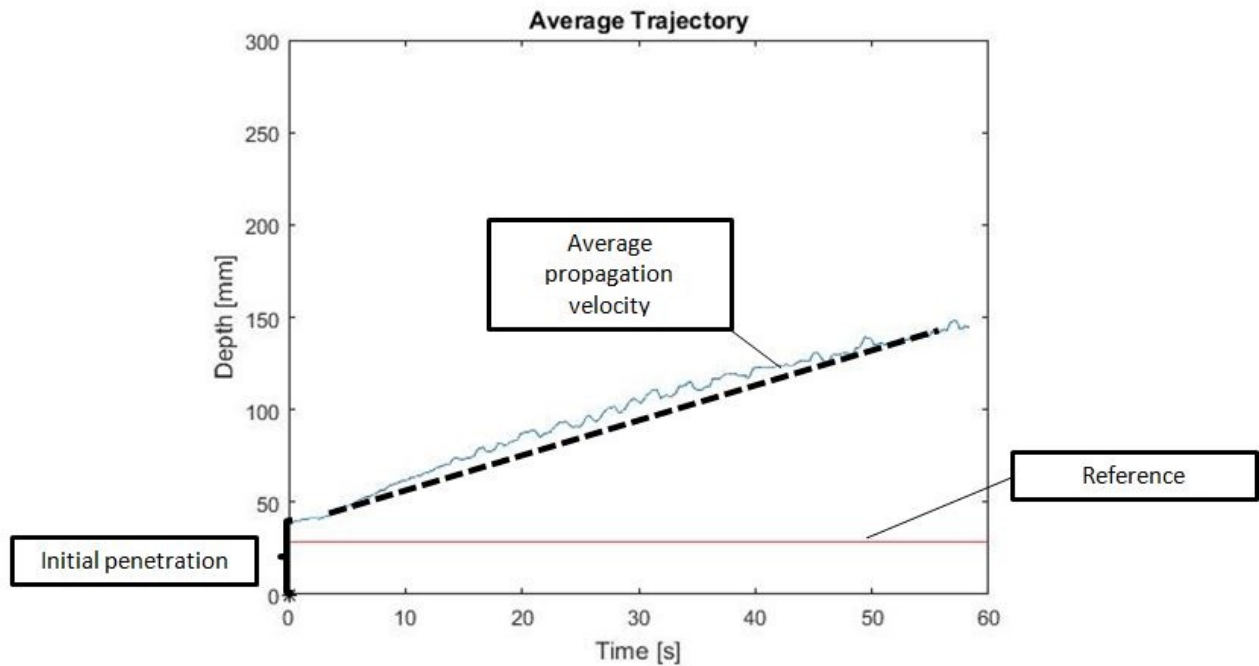
Fig. 15.   Definition of terms used to describe the different phases of the penetration trajectory. The initial penetration is the first second of the experiment. The average propagation velocity is an average velocity calculated between 10% and 90% of the run. The reference line shows the result of the experiment when no airflow is used.
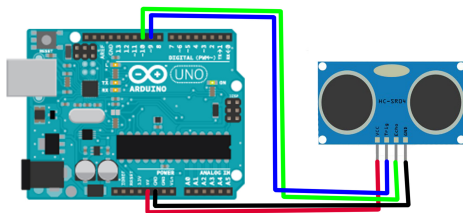
Fig. 16.   The connection scheme of the Arduino Uno and the ultrasound distance sensor.

TABLE I
EXPERIMENTAL CONDITIONS OF EXPERIMENT 1.

Experiment 1	Diameter [μm]	Airflow [l/min]	Mass [kg]
Condition 1	40-70	25	0.8
Condition 2	40-70	25	1.3
Condition 3	40-70	25	1.8
Condition 4	40-70	25	2.3
Condition 5	150-250	25	0.8
Condition 6	150-250	25	1.3
Condition 7	150-250	25	1.8
Condition 8	150-250	25	2.3

airflow was in its steady state, the tool was lowered to the surface level. The Arduino Uno was turned on, and the data acquisition was started. The penetration tool was then released, and a timer was started. Each run ends if the tool has reached a depth of $150\ mm$ or if 60 seconds had passed. For each configuration, a reference measurement was taken without the airflow. At the end of each run, the ultrasound sensor was cleaned as airborne glass beads can fill the sensor and block the signal.

2) Experiment 2: variation of airflow: For the second experiment, the mass of the penetration tool was held constant at the tools' mass of $0.8\ kg$. The airflow was varied between $25\ l/min$ and $100\ l/min$. These airflows are based on a pilot experiment that showed that a lower airflow did not result in any fluidizing effect and airflow above $100\ l/min$ caused excessive dust formation. In total four different airflows were used: $25\ l/min, 50\ l/min, 75\ l/min,$ and $100\ l/min$. Every configuration was repeated six times. Table II lists the experimental conditions.

The procedure for Experiment 2 was mainly the same as the one described for Experiment 1, with some small alterations. There was no additional mass loaded onto the penetration tool, but the airflow was set to either $25\ l/min, 50\ l/min, 75\ l/min,$ or $100\ l/min$. The order of testing was randomised for the airflow condition. For Experiment 2, no reference data without airflow were collected as these were identical to the reference data of Experiment 1 without additional mass.

C. Results

The raw data of Experiment 1 and 2 can be found in Appendix A: Raw Data. Figure 17 shows the average trajectories for the first experiment. The average depth was
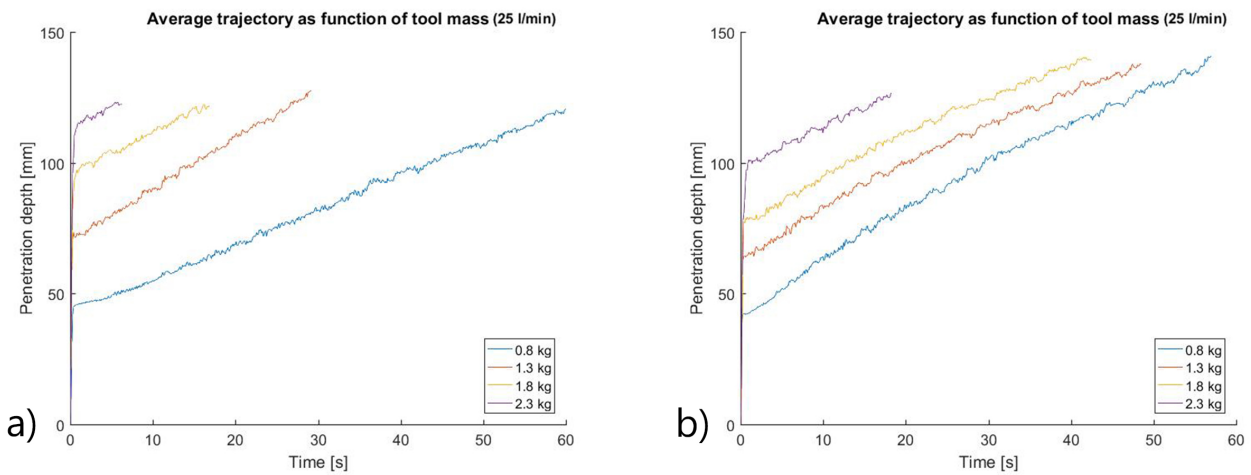
Fig. 17.   Average trajectory of six runs of every mass configuration using glass beads of a) $40 - 70\ \mu m$ and b) $150 - 250\ \mu m$.
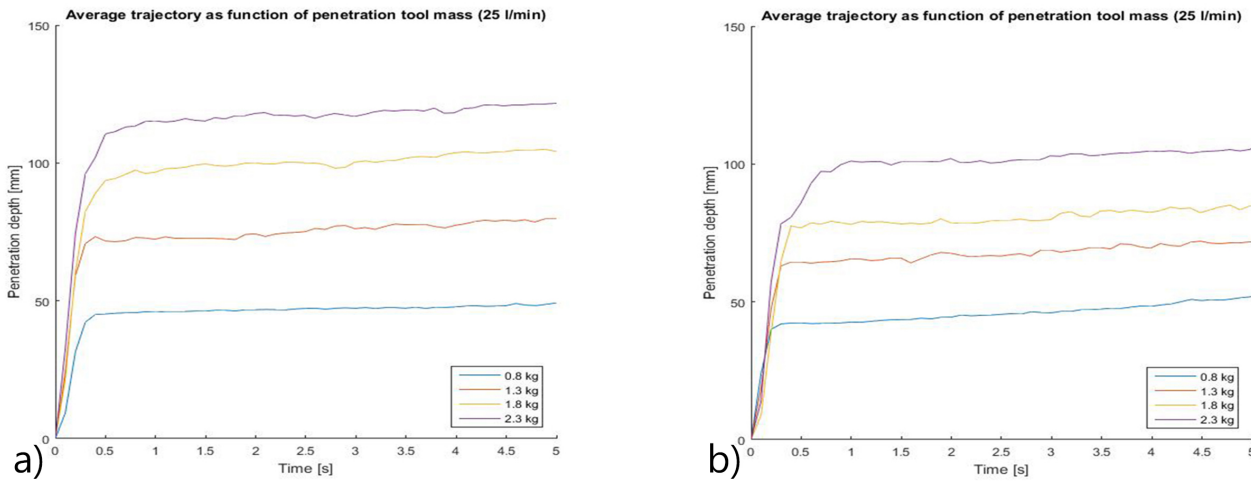
Fig. 18.   Close-up of the initial penetration using glass beads of a) $40 - 70\ \mu m$ and b) $150 - 250\ \mu m$.
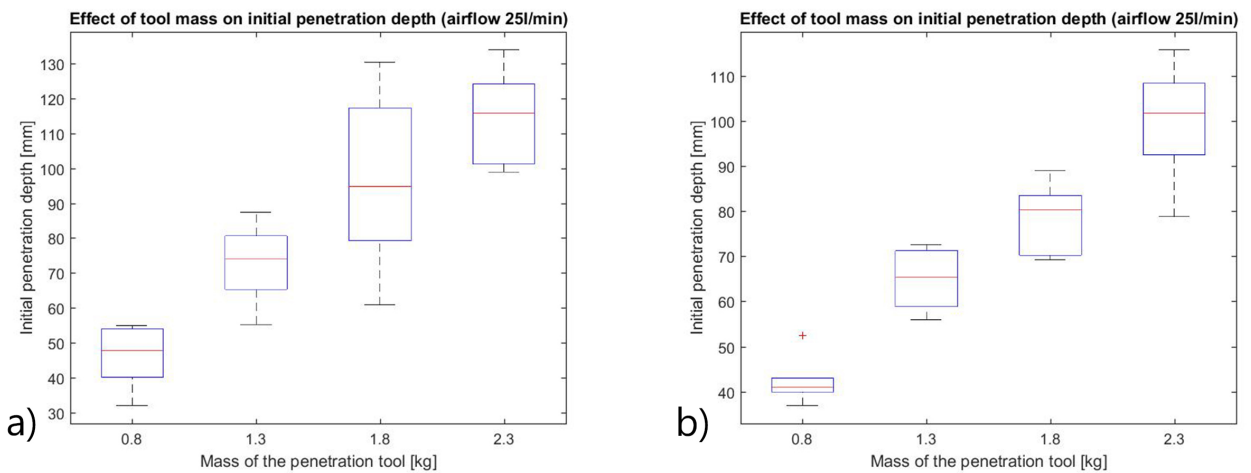
Fig. 19.   Boxplot of the initial penetration while varying the mass of the penetration tool using glass beads of a) $40 - 70\ \mu m$ and b) $150 - 250\ \mu m$.
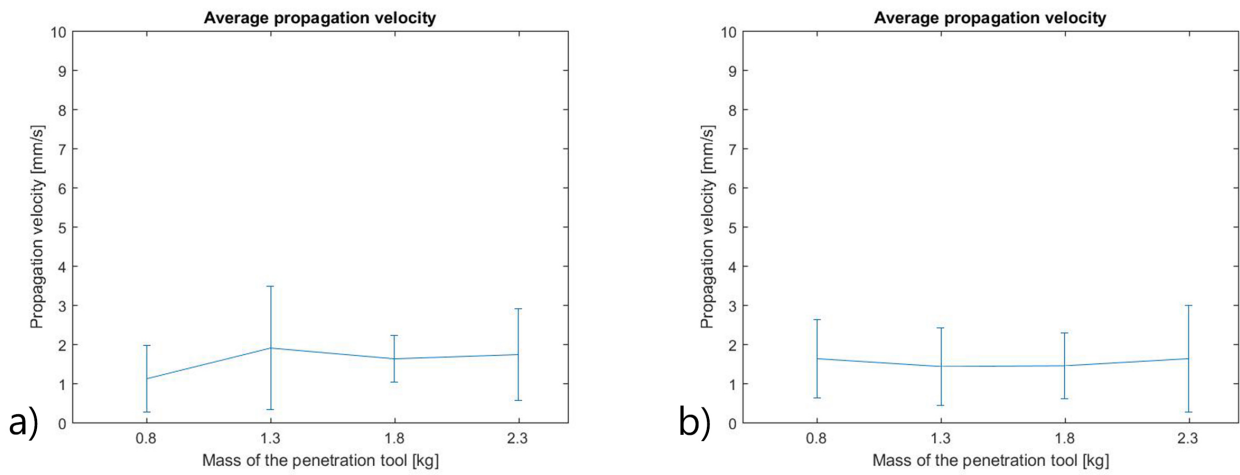
Fig. 20.   The propagation velocity as a function of penetration tool mass using glass beads of a) $40 - 70 \; \mu m$ and b) $150 - 250 \; \mu m$. Error bars show minimum and maximum values.
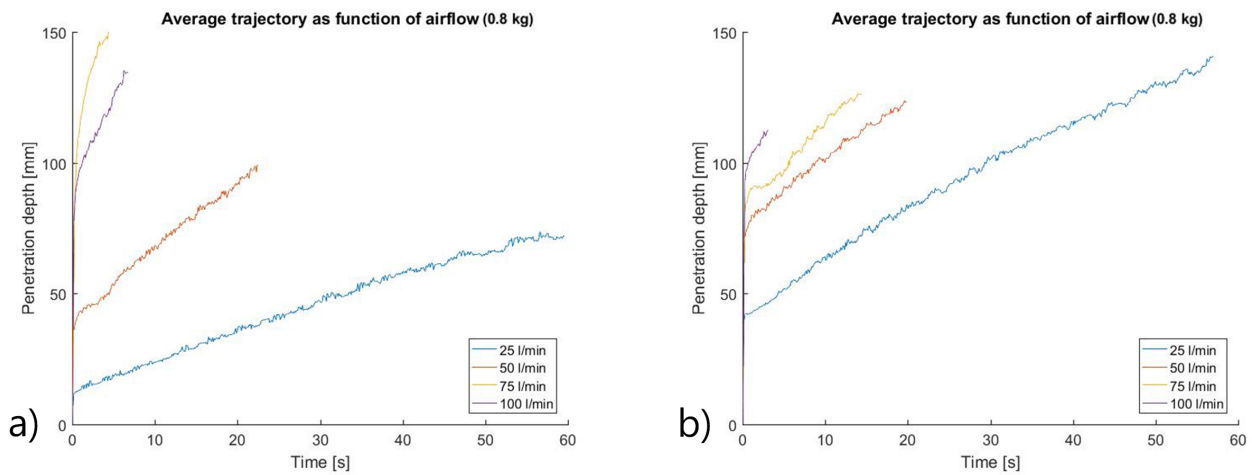
Fig. 21.   Average trajectory of six runs of every airflow configuration using glass beads of a) $40 - 70 \; \mu m$ and b) $150 - 250 \; \mu m$.
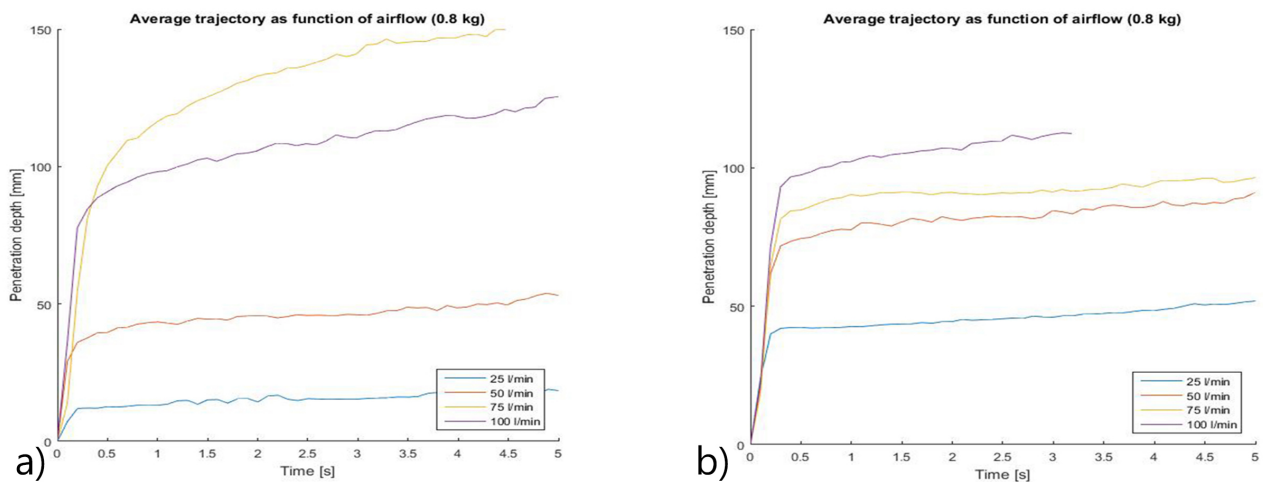
Fig. 22.   Close-up of the initial penetration using glass beads of a) $40 - 70 \; \mu m$ and b) $150 - 250 \; \mu m$.
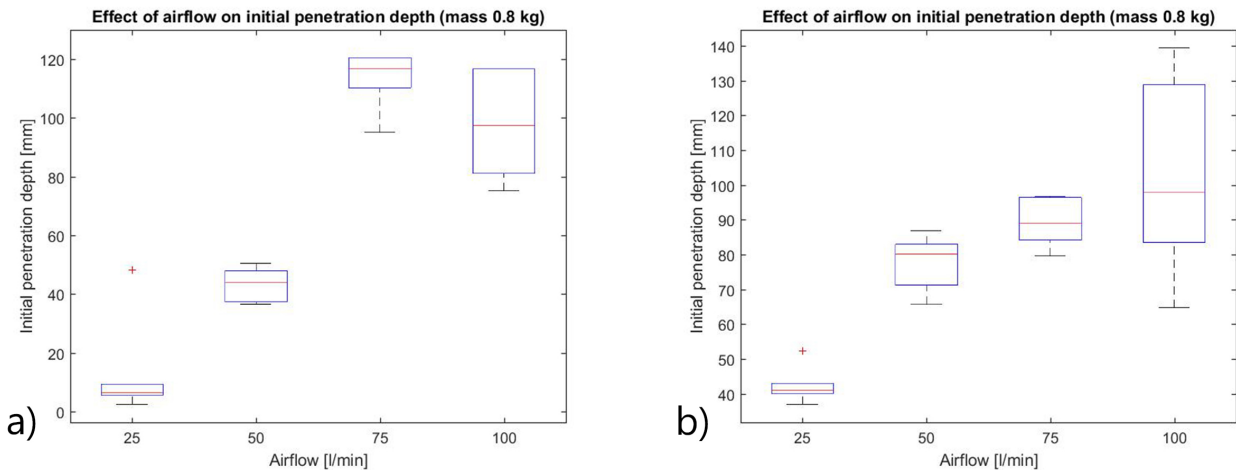
Fig. 23.   boxplot of the initial penetration while varying the airflow using glass beads of a) $40-70\ \mu m$ and b) $150-250\ \mu m$.

TABLE II

EXPERIMENTAL CONDITIONS OF EXPERIMENT 2.

Experiment 2	Diameter [µm]	Airflow [l/min]	Mass [kg]
Condition 1	40-70	25	0.8
Condition 2	40-70	50	0.8
Condition 3	40-70	75	0.8
Condition 4	40-70	100	0.8
Condition 5	150-250	25	0.8
Condition 6	150-250	50	0.8
Condition 7	150-250	75	0.8
Condition 8	150-250	100	0.8

calculated until the end of the shortest repetition (see Appendix D: Averaging Example). Figure 18 focuses on the first 5 seconds, showing the initial penetration in detail.

For the Class A glass beads, the initial penetration is $46\ mm$ at $0.8\ kg$, $73\ mm$ at $1.3\ kg$, $96\ mm$ at $1.8\ kg$, and $115\ mm$ at $2.3\ kg$. Only the differences between $1.3\ kg$ and $1.8\ kg$ (p-value 0.08) and between $1.8\ kg$ and $2.3\ kg$ (p-value 0.21) are not significant. For the Class B glass beads the initial penetration averages $42\ mm$ at $0.8\ kg$, $65\ mm$ at $1.3\ kg$, $79\ mm$ at $1.8\ kg$, and $100\ mm$ at $2.3\ kg$. With the exception of the increase from $65\ mm$ to $79\ mm$ (p-value 0.065) these results are significant. This data also shows a consistent lower initial penetration when compared to Class A beads (Table III). The decrease in

TABLE III

COMPARISON BETWEEN THE AVERAGE INITIAL PENETRATION USING

CLASS A AND CLASS B GLASS BEADS.

Tool mass [kg]	Class A depth[mm]	Class B depth[mm]	p-value
0.8	46	42	0.40
1.3	73	65	0.18
1.8	96	79	0.13
2.3	115	100	0.079

initial penetration between Class A and B glass beads is not significant. The boxplot in Figure 19 visualises the initial penetration for both substrates.

The propagation velocity after the initial penetration is shown in Figure 20. When using Class A glass beads, the propagation velocity seems to increase when the mass of the penetration tool increases. This increase is significant when we compare $0.8\ kg$ to $1.3\ kg$ (p-value 0.0069) and when we compare $0.8\ kg$ to $2.3\ kg$ (p-value 0.039). When using the Class B glass beads, no significant change in propagation velocity can be observed when changing the penetration tool mass.

In Figure 21, the averages of six repetitions are shown for, respectively, the experiments with the Class A and Class B glass beads. Figure 22 focuses on the first five seconds, showing the initial penetration in detail. For Class A glass beads, the initial penetration averages $13\ mm$ at $25\ l/min$, $43\ mm$ at $50\ l/min$, $114\ mm$ at $75\ l/min$, and $97\ mm$ at $100\ l/min$. This data shows a positive relation between airflow and initial penetration depth with significant results between all averages except between $75\ l/min$ and $100\ l/min$ (p-value 0.26). For Class B glass beads, the initial penetration averages $42\ mm$ at $25\ l/min$, $78\ mm$ at $50\ l/min$, $89\ mm$ at $75\ l/min$, and $102\ mm$ at $100\ l/min$. These results also show a positive relation between penetration depth and airflow. However, the results are only significant when comparing them to the lowest airflow condition of $25\ l/min$ (p-values: 1. $50\ l/min$ p=0.0037, 2. $75\ l/min$ p $=1.98*10^{-4}$, 3. $100\ l/min$ p=$8.53*10^{-6}$). A boxplot of the initial penetration while using both substrates is shown in Figure 23. The substrate depth of this experiment was insufficient to calculate a propagation velocity accurately. Especially at an airflow of $75\ l/min$ and $100\ l/min$ there was no clear distinction between initial penetration and propagation.

V. EXPERIMENTAL EVALUATION: THE EFFECT OF DEPTH ON THE PENETRATION TRAJECTORY
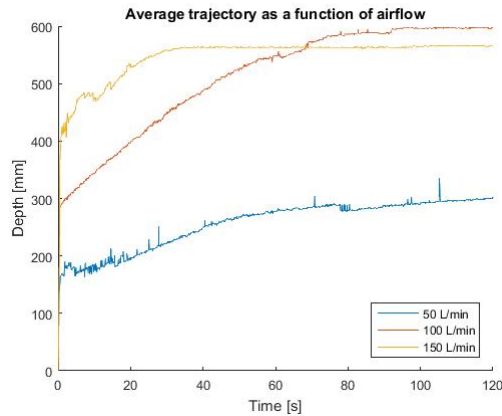
Fig. 24. Average trajectory of six runs of every configuration using glass beads of $150 - 250 \ \mu m$ and the reference data.
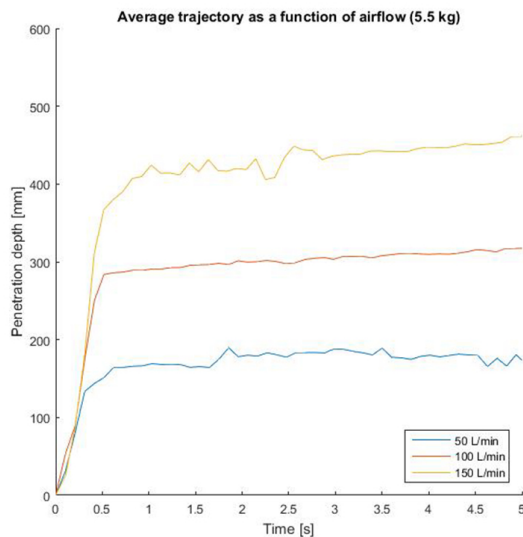
Fig. 25. Close-up of the initial penetration using glass beads of $150 - 250 \ \mu m$.

A. Data acquisition and analysis

The data acquisition during Experiment 3 was identical to the first two experiments described in Section IV-A. A ultrasound distance sensor was connected to an Arduino Uno which sent the measured depth to a computer. Because of the added height, the maximum time of a trial was extended to two minutes. This required some changes in the data analysis. The used Matlab scripts can be found in Appendix B: Matlab. To analyse the significance of the results a one-way ANOVA was used and their p-values are given.
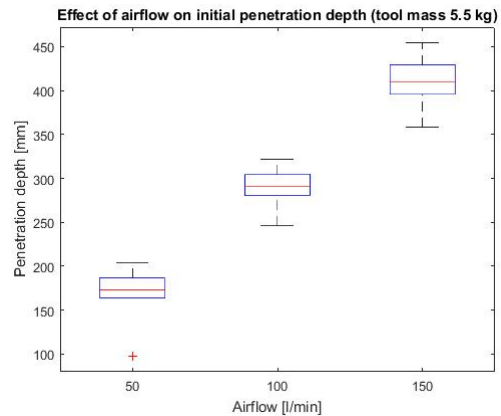
Fig. 26. Boxplot of the initial penetration using glass beads of $150 - 250 \ \mu m$.

B. Procedure

The mass of the penetration tool in the third experiment was held constant at $5.5 \ kg$. This mass was due to the weight of the vertical guidance and no additional mass was added. The independent variable for this experiment was the airflow. The airflow was varied between $50 \ l/min, 100 \ l/min$, and $150 \ l/min$. The order of testing was randomised for the airflow condition. Every configuration was repeated six times. Table IV lists the experimental conditions.

TABLE IV
EXPERIMENTAL CONDITIONS OF EXPERIMENT 3.

Experiment 3	Diameter[μm]	Airflow [l/min]	Mass [kg]
Condition 1	150-250	50	5.5
Condition 2	150-250	100	5.5
Condition 3	150-250	150	5.5

At the start of each experiment, the substrate was levelled. The airflow was initiated at a height relative to the surface of $200 \ mm$. When the airflow was in its steady state, the tool was lowered to the surface level. The Arduino Uno was turned on, and the data acquisition was started. The penetration tool was then released, and a timer was started. Each repetition ends if the tool had reached a depth of $1000 \ mm$ or when 120 seconds had passed. A reference measurement was recorded without the airflow. At the end of each repetition, the ultrasound sensor was cleaned.

C. Results

The raw data of Experiment 3 can be found in Appendix A: Raw Data. Figure 24 shows the averages of all six repetitions at each condition. Figure 25 zooms in on the initial penetration. The average initial penetration increased from $166 \ mm$ at $50 \ l/min$, to $289 \ mm$ at $100 \ l/min$, and to $410 \ mm$ at $150 \ l/min$. The initial penetration increased with $123 \ mm$ between $50 \ l/min$ and $100 \ l/min$ and $244 \ mm$ between $50 \ l/min$ and $150 \ l/min$ (p-values $2.09 * 10^{-5}$ and $4.42 * 10^{-9}$). The boxplot in Figure 26 focuses on

this increase and shows the median and spread of the data. The minimum penetration depth at 50 l/min is 98 mm and its maximum is 204 mm. At an airflow of 100 l/min the minimum penetration depth increased to 246 mm and the maximum increases to 322 mm. For the airflow of 150 l/min we see an increase of the minimum to 359 mm and the maximum increases to 454 mm.

After the initial penetration, the tool continued to propagate deeper into the substrate. With an airflow of 50 l/min, no steady state was reached after 120 s. The average depth at this point was 302 mm. At an airflow of 100 l/min, the steady state was reached after approximately 93 s at a depth of 595 mm. The average of the 150 l/min condition reached its steady state at approximately 34 s at a depth of 563 mm. The final penetration with an airflow of 50 l/min is significantly different from the results of both 100 l/min and 150 l/min (p-value $1.70 * 10^{-6}$ and $6.40 * 10^{-6}$). On average, the final penetration of 100 l/min is deeper than at 150 l/min, but this result is not significant (p-value 0.68).

VI. FLUGRAB: CONCEPT DESIGN

A. Grab design parameters

For the conceptual design, some basic grab design parameters are defined. These parameters are based on the characteristics of grabs currently built for the transhipment of wheat (Table V). The blade lip length is important as the

TABLE V

DESIGN PARAMETERS FOR THE CONCEPT GRAB.

Grab parameters	
Blade lip length	8000 mm
Weight	10,000 kg
Volume	35 m³
Bulk density	700 kg/m³

penetration tool results will be scaled to this length.

B. Basic design choices

Based on the results of the experiments, design choices can be made. An essential one is the usage of the fluidization principle. Fluidization can be used in two ways. One method is to use fluidization to increase the initial penetration of the grab. Another method is to use fluidization both during the initial penetration until the steady state depth is reached. Using fluidization only in the initial penetration stage has the advantage of using pressurised air for only a short period. When using high airflow, more than half of the increase in penetration depth occurs in the first second. When the full effect of fluidization is used, the air requirement increases to $30 - 100$ s depending on the airflow.

The second choice concerns the grab design. Either a design can be made from scratch, or an existing grab can be adjusted to use the fluidization principle. The benefit of creating a new design is the lack of restrictions that adjusting a current design brings. This design freedom could lead to

an optimised result. However, at this stage of the research, it would require more data before a new design can be made. Adjusting an existing design has the added benefit of being easily comparable to a current grab. An adjusted design would show the effect of the addition of fluidization without the potential effect of the different design. When a current design is adapted a choice has to be made between the Scissor grab or the Clam-shell grab.

The last choice is where to place, generate, and store the compressed air. There are two possibilities: either this is done on the grab itself, or outside the grab. Placing the generation and storage of compressed air on the grab itself has the benefit of only adapting the grab and leaving the surroundings unchanged. This makes implementation less complex. The localised generation and storage would add weight to the grab making its dimensions critical. Placing the generation and storage of compressed air outside of the grab would remove most of the dimension and weight limitations. However, this introduces the problem of distributing the air from the point of generation to the grab.

C. Use of the fluidization principle

The total air requirement per cycle can be calculated with the following equations:

$$V = S\dot{Q}t \tag{11}$$

$$S = \frac{\ell_{real}}{\ell_{tool}} \tag{12}$$

Where S is the scaling factor calculated by dividing the length of a real sized blade lip (ℓ_{real}) by the length of the penetration tool (ℓ_{tool}). $\dot{Q}$ is the airflow per second used in the experiments, and t is the time in seconds the fluidization is used. This results in V, the total volume of air under normalised conditions.

As only the time differs between the two situations, the volume of air needed is directly proportional to the time. For a scaled airflow of 150 l/min, this results in a usage of 285 l when fluidization is used for the initial penetration, and 8550 l of air when it is used during the entire digging cycle. The increase in air requirement does not justify the increase in the total penetration depth. For the concept design, only using fluidization to increase initial penetration is therefore recommended.

D. Adjusting the current grab design or creating a new design

On the long-term, creating a new grab design dedicated to the fluidization principle is most interesting. However, in order to achieve this, more research into the fluidization grab principle needs to be done. To observe the benefits of fluidization on the short-term, it is beneficial to adjust a current grab design.

The Clam-shell grab is most suited to adjust for designing a concept. The Clam-shell grab is much lighter than the Scissor grab and would benefit more from the weight reduction that can be achieved using the fluidization principle.
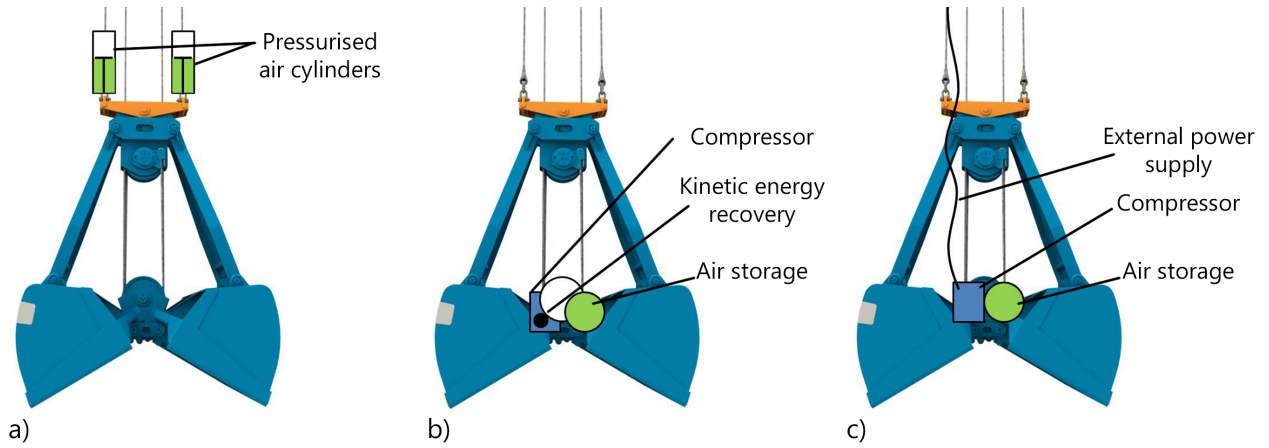
Fig. 27. The three concept designs. The storage of compressed air is shown in green. a) The first concept uses two cylinders filled with air. The cylinders are pressurised by the mass of the grab when the grab is hoisted, and release on touching down on the substrate. b) The second concept uses a compressor (blue square) that fills a pressurised air storage with the use of energy recovered from lowering the grab. The white circle represents a rope sheave where the energy, released by lowering the grab, is used to power the compressor. c) The third concept also uses a compressor (blue square) and air storage, but the compressor is powered from an external source.

E. Generation and storage of compressed air

Due to the choice of only using fluidization during the initial penetration, generation and storage of compressed air can be fitted onto the grab. Commercial compressor systems that fulfil the storage and generation criteria can be lighter than $50\ kg$, like the Airpress HL 425-50 [39]. A compressor would not be the only option to generate the required compressed air.

During brainstorm sessions with employees of NEMAG B.V. several options for the implementation of fluidization in a grab were discussed. During these sessions it was brought up that, during a grab cycle, a considerable amount of energy is lost by braking when lowering the grab. If this energy is used, no external power source or compressor is needed. Using a T-s diagram for air, we can calculate the enthalpy difference between air with an absolute pressure of 1 bar and at 5 bar. Assuming reversible compression, the enthalpy difference is $170\ kJ/kg$ and the mass of $300\ l$ of air at 1 bar equals $0.43\ kg$. This results in an energy requirement for the compression of $73\ kJ$ per cycle. The potential energy lost when lowering a grab of $10,000\ kg$ for $5\ m$ equals $10,000 \cdot 9.81 \cdot 5 = 0.5\ MJ$. Theoretically, it is possible to design a system that recovers part of the potential energy of the grab to generate the compressed air.

Another possibility is to use the weight of the grab to pressurise the air. Pistons inside of cylinders, between the grab and the hoisting ropes, can pressurise air while the grab is lifted, and release this pressurised air when the grab is placed on the substrate. In this way the required power is delivered by the crane without the need of power cables running from the crane to the grab. For this concept the cylinders need a volume of $300\ l$ and the maximum pressure difference is 4 bar. The dimensions of the cylinders can be calculated using the following equations:

$$F_p = PA \tag{13}$$

Where P is the pressure difference of 4 bar ($400.000\ Pa$) and A the combined area of the pistons of the cylinders. The force F_p now has to be equal to the gravitational force acting on the grab:

$$F_z = mg \tag{14}$$

With m the mass of the grab and g the gravitational acceleration. Combining Equation 13 and 14, results in a maximum area of the cylinders of $0.245\ m^2$. Because the minimum volume is known, the following equations are used to obtain the dimensions of the cylinders:

$$A = 2\pi r^2 \tag{15}$$

$$V = Ah \tag{16}$$

Where r is the radius of the cylinder, h the height of the cylinder and V the specified volume of $300\ l$. Using Equations 15 and 16, results in a radius of the piston of $0.198\ m$ and a height of $1.22\ m$.

F. Potential concepts of the FluGrab

The design choices in the previous sections result in three concept designs based on the Clam-shell grab (Figure 27). Concept a) uses the weight of the grab to pressurise air inside two cylinders on top of the grab when it is lifted. This air is released when the grab is placed on top of the substrate. Concept b) uses the energy that is released when the grab is lowered in order to power a compressor, which in turn fills the air storage. Concept c) uses a compressor and air storage, but the compressor is powered from an external source.

To make a choice between the concepts, a Harris profile is made (Table VI). The concepts are assessed based on their required adjustments to the grab design, required external adjustments (e.g. crane / ship / shore), their feasibility based on the calculations made in Section VI-E and the extent to which the solution is innovative.

In the Harris profile, - - means the concept scores below the requirements. - Means the requirement poses a (technical) challenge. + Means the concept fulfils the requirement. ++ Means a the concept exceeds the requirements.

TABLE VI

HARRIS PROFILE

	Concept a	Concept b	Concept c
Adjustments grab	-	-	+
External adjustments	+	++	--
Feasibility	-	+	++
Innovation	+	++	-

Concept a) and b) both need significant adjustments to the grab. Concept a) needs large cylinders on top of it to compress the air. Concept b) needs to adjust the rope sheaves to make energy recovery possible in addition to installing a compressor and air storage. Concept c) needs a compressor and air storage so in terms of adjustments to the grab, concept c) performs best.

Concept b) needs no external adjustments. Concept a) makes the grab over a meter taller, which could require some adjustments if the maximum hoisting height of the crane is insufficient. Concept c) needs an external power supply, relying on adjustments made outside the grab itself.

The feasibility of concept a) scores best, as the power is supplied from an external source. The calculations in Section VI-E show there is enough energy to power the compressor when the grab is lowered. Therefore, concept b) is feasible as well. Concept c) requires large cylinders to compress the air, making it the least feasible solution.

Concept b) has a maximum score in innovation as the solution is compact, simple, and independent of external sources at the same time. Although concept a) is independent of external sources and is simple, it is not compact. Furthermore the dimensions of the cylinders are heavily dependent on the mass of the grab. If the grab is made lighter, the cylinder has to be made taller to reduce the area of the piston. Concept c) is compact and simple, but needs an external power supply. Taking all four rating points into account, concept b) scores best.

VII. DISCUSSION

A. *Interpretation of the experiments*

Figure 28 shows the situation around the penetration tool. The air forms a boundary layer around the penetration tool where the air-velocity is high, and the substrate is fully fluidized.

The first experiment is conducted to show the influence of penetration tool mass on initial penetration depth and propagation velocity. We hypothesised that the initial penetration increases with increasing penetration tool mass. Figure 19 shows that there is a linear proportional relation between initial penetration and tool mass and the results are statistically significant. Comparing the results of both
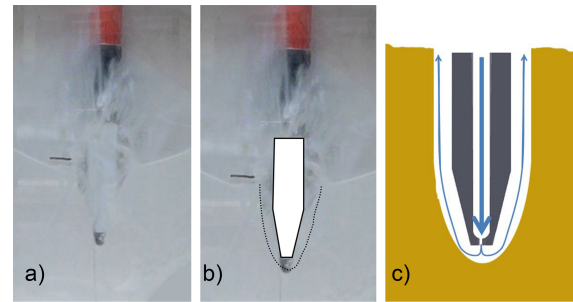
Fig. 28. Model of the fluidization around the penetration tool. a) The unedited camera footage. b) Outlines of the tool and substrate/air boundary are added. c) A schematic view with the substrate (yellow) and arrows showing the direction of the airflow (blue).

substrates we see slightly lower average initial penetration depths when using the Class B glass beads ($150 - 250\ \mu m$) compared to Class A glass beads ($40 - 70\ \mu m$). This is an expected effect, as, according to the Geldart classification of particles, these particles require more effort (e.g. higher airflow) to fluidize [26]. Furthermore, the increased particle size increases the permeability of the substrate. An increased permeability means that more air can escape through the substrate, instead of through the boundary layer around the penetration tool.

For the propagation velocity, it was hypothesised that an increase in penetration tool mass meant the penetration velocity would also increase. The hypothesis was based on the theory of effective viscosity. The geometry of the tool did not change, but the gravitational forces on the penetration tool increased. As a result, we expected a higher propagation velocity. The result of this experiment is shown in Figure 20. Although the experiment with Class A glass beads showed an increase in average propagation velocity, the difference is not significant. Experiments using glass beads of Class B did not show any relation between the parameters and the average propagation velocity of the four testing conditions were not significantly different. Apparently, in the tested range, the mass of the penetration tool is not a dominant variable for the propagation velocity. A possible explanation is that the airflow needs time to clear the path for the tool and fluidize the surroundings, and therefore adding more pressure to the substrate does not aid in this process.

In the second experiment, the influence of airflow on the initial penetration and propagation velocity is investigated. It was hypothesised that an increase in airflow increases the initial penetration and propagation velocity. The hypotheses were based on the theory of effective viscosity (Section II-C). A higher airflow leads to a higher void fraction and thus, to a lower effective viscosity. Figure 23 shows the effect on the initial penetration depth. Using both Class A and B glass beads the data shows a linear proportional relation between these parameters. The difference between $25\ l/min$ and $50\ l/min$ was in both cases significant, and the data were clear for these settings. With higher airflow, the data were less consistent resulting in a higher spread. This also

explains the unexpected peak at $75 \ l/min$ in the experiment with glass beads of Class A. It is expected that the average of this data would be between the averages of $50 \ l/min$ and $100 \ l/min$. These results suggest there is a positive relation between airflow and initial penetration depth.

The third experiment gives information about the influence of depth on the penetration trajectory. We hypothesised that with increasing depth, the penetration velocity would decrease. Figure 24 shows a decline in propagation velocity as the penetration depth increases. Eventually, the penetration velocity goes to zero. The observed decline in propagation velocity confirms the hypothesis. An increase in airflow does not seem to change the depth of this steady state but does seem to quicken the convergence to this point. Looking to the theory in Section II-B this can be explained by the increase in internal friction for deeper particles. Not all the particles are fluidized in the enclosure, only those close to the penetrating tool. This means that not all the stress chains are interrupted. Possible solutions to increase the final depth include a new nozzle design, higher air pressure or an even higher airflow.

The increased height of Experiment 3 also gave us the opportunity to measure the initial penetration at a higher airflow. This data was obtained during the experiments to measure propagation velocity. The data were summarised in Figure 26 and shows a significant increase in initial penetration depth with increasing airflow. In the tested range of $50 \ l/min \ - \ 150 \ l/min$, the relation seems to be linear proportional.

B. Limitations of the study

1) Substrate choice consequences: In this work glass beads are used as a substrate for the experiments. The well-defined properties of glass beads make them ideal for experiments, but there are some downsides to their use. Glass beads are often better defined regarding size and shape than common bulk materials. A bulk material does not necessarily fall completely inside the boundaries of one Geldart class. This can result in a substrate that does not completely fluidize and chunks of material that block further propagation. The experimental set-up used in this work was not able to fluidize particles of Class D according to the Geldart classification of particles. Therefore we had to limit the experiments to Class A and B particles. This limits our ability to give design recommendations outside this range of particle sizes.

2) Wall effects and 2D simplification: Although we tried to reduce wall effects as far as possible, there are wall effects caused by the 2D representation of the experiments. A part of the air passed between the Plexiglas and penetration tool. On the actual scale of a grab, this would be considerably less due to the length of the blade lip on a grab. This can possibly reduce the amount of air needed for penetration.

3) The effects of friction: In a free digging environment there is, besides the resistance of the substrate, no friction with the external world. In the experimental set-up, the friction forces are reduced by constructing the enclosure with smooth surfaces and using a well-lubricated guidance system. Although this minimised the effect of friction, it did not

eliminate it. The resulting friction forces can have reduced propagation velocities and penetration depths.

4) The effects of scaling: The penetration tool is based on the dimensions of an actual blade lip to reduce scaling effects. However, the pressure on the blade lip is scaled down. In an actual Clam-shell grab the weight of the grab per unit of length of the blade lip is in the order of $1 \ kg/mm$. Scaling this would result in a required mass of the penetration tool of $70 \ kg$. Constructing a penetration tool of $70 \ kg$ is an unfeasible scenario as it would greatly increase the initial penetration during the test. This would require even deeper enclosures in which to test. Taking this into consideration, the mass of the penetrating tool is scaled down to respectively $0.8 \ kg$ for the first two experiments and to $5.5 \ kg$ for the third experiment.

C. Future work and recommendations

Based on the findings of this work it would be interesting to continue the research using more substrates. Based on their Geldart classification, alumina and ilmenite show potential to be tested in the FluGrab design. Another type of research can be done to explore the requirements for Class D particles to be included in the range of substrates.

In the third experiment, the fluidization did not seem to work more than $600 \ mm$ below the surface of the substrate. Further research is necessary to increase the working depth of the fluidization principle and to get a better understanding why this limitation exists in the current set-up. Possible parameters to vary would be air pressure, airflow, or the nozzle design.

Based on the limitations of this work it is useful to experiment on a larger scale, for example with a grab with blade lips of a meter wide to reduce the wall effects. When this is performed in a Clam-shell like set-up, linear guidance can be removed, decreasing the effects of friction. Further, it would create a situation closer to the reality with a more realistic closing trajectory of the shells. While currently, the co-simulation between granular materials and fluid flows is extremely hard, simulation of the FluGrab would allow for a full sized test of the principle before a FluGrab is built.

The variance of the experimental data can be improved in future work by replacing the "In Line Floating Ball Flow Meter" for a digital airflow controller. The analogue sensor made accurately controlling the airflow difficult. Therefore an accurate digital sensor can contribute to more consistent data.

VIII. CONCLUSION

Using the bio-inspired approach, the *Octopus kaurna* was used as inspiration for the investigation of a new grab working principle. It was found that an increase in penetration tool mass and an increase in airflow both increase the initial penetration of the penetration tool. An increase in airflow also increased the propagation velocity of the penetration tool. The principle of fluidization can increase the initial penetration of a grab by 200% using $285 \ l$ of air for the tested substrates. The increase in initial penetration

can solve the efficiency reduction for light grabs, further reducing the mass of future grabs while maintaining its digging properties. Calculations made for the concept design show the possibility of using the potential energy of the grab to compress air for the fluidization. The concept designed in this work uses this possibility. The FluGrab concept consist of a energy recovery system that powers a compressor in order to pressurise the air needed for fluidizing the substrate. The main advantages of the concept are the independence of external sources, the lack of adjustments outside of the grab and its compactness. In conclusion, this work showed that the application of fluidization in a grab is a promising approach to reduce the mass of a grab, while maintaining its digging capabilities.

ACKNOWLEDGMENT

REFERENCES

[1] F. Verantius, *Machinae Novae*, 1605.

[2] "Clamshell grab," http://www.nemag.com/en/products/clamshell-grab, Nemag BV, last visited: 20-4-2017.

[3] "Nemag bv products," https://www.nemag.com/solutions/, Nemag BV, last visited: 3-11-2017.

[4] J. Finn and M. Norman, "Southern sand octopus," *Taxonomic Toolkit for marine life of Port Phillip Bay*, 2011, last visited: 28-11-2017.

[5] J. Montana, J. K. Finn, and M. D. Norman, "Liquid sand burrowing and mucus utilisation as novel adaptations to a structurally-simple environment in octopus kaurnastranks, 1990," *Behaviour*, vol. 152, no. 14, pp. 1871–1881, 2015.

[6] S. W. Lommen, "Virtual prototyping of grabs," Ph.D. dissertation, TU Delft, 2016.

[7] K. M. Dorgan, C. J. Law, and G. W. Rouse, "Meandering worms: mechanics of undulatory burrowing in muds," *Proceedings of the Royal Society of London B: Biological Sciences*, vol. 280, no. 1757, p. 20122948, 2013.

[8] K. M. Dorgan, "The biomechanics of burrowing and boring," *Journal of Experimental Biology*, vol. 218, no. 2, pp. 176–183, 2015.

[9] A. Hosoi and D. I. Goldman, "Beneath our feet: strategies for locomotion in granular media," *Annual Review of Fluid Mechanics*, vol. 47, pp. 431–453, 2015.

[10] R. D. Maladen, Y. Ding, C. Li, and D. I. Goldman, "Undulatory swimming in sand: subsurface locomotion of the sandfish lizard," *science*, vol. 325, no. 5938, pp. 314–318, 2009.

[11] A. Zundelevich, B. Lazar, and M. Ilan, "Chemical versus mechanical bioerosion of coral reefs by boring sponges-lessons from pione cf. vastifica," *Journal of experimental biology*, vol. 210, no. 1, pp. 91–96, 2007.

[12] S. S. Sharpe, S. A. Koehler, R. M. Kuckuk, M. Serrano, P. A. Vela, J. Mendelson, and D. I. Goldman, "Locomotor benefits of being a slender and slick sand swimmer," *Journal of Experimental Biology*, vol. 218, no. 3, pp. 440–450, 2015.

[13] A. G. Winter, R. L. Deits, and A. E. Hosoi, "Localized fluidization burrowing mechanics of ensis directus," *Journal of experimental biology*, vol. 215, no. 12, pp. 2072–2080, 2012.

[14] E. Trueman, A. Brand, and P. Davis, "The dynamics of burrowing of some common littoral bivalves," *Journal of Experimental Biology*, vol. 44, no. 3, pp. 469–492, 1966.

[15] S. M. Stanley, *Relation of shell form to life habits of the Bivalvia (Mollusca)*. Geological Society of America, 1970, vol. 125.

[16] R. Cocco, S. R. Karri, T. Knowlton *et al.*, "Introduction to fluidization," *Chemical Engineering Progress*, vol. 110, no. 11, pp. 21–29, 2014.

[17] J. R. van Ommen and N. Ellis, "Fluidization," https://www2.msm.ctw.utwente.nl/sluding/, 2010, last visited: 12-11-2017.

[18] C. Wen and Y. Yu, "A generalized method for predicting the minimum fluidization velocity," *AIChE Journal*, vol. 12, no. 3, pp. 610–612, 1966.

[19] Geotechdata.info, "Soil permeability coefficient," http://www.geotechdata.info/parameter/permeability.html, last visited: 6-11-2017.

[20] N. Frankel and A. Acrivos, "On the viscosity of a concentrated suspension of solid spheres," *Chemical Engineering Science*, vol. 22, no. 6, pp. 847–853, 1967.

[21] I. M. Krieger and T. J. Dougherty, "A mechanism for non-newtonian flow in suspensions of rigid spheres," *Transactions of the Society of Rheology*, vol. 3, no. 1, pp. 137–152, 1959.

[22] v. H. Eilers, "Die viskosität von emulsionen hochviskoser stoffe als funktion der konzentration," *Colloid & Polymer Science*, vol. 97, no. 3, pp. 313–321, 1941.

[23] F. Ferrini, D. Ercolani, B. De Cindio, L. Nicodemo, L. Nicolais, and S. Ranaudo, "Shear viscosity of settling suspensions," *Rheologica Acta*, vol. 18, no. 2, pp. 289–296, 1979.

[24] S. H. Maron and P. E. Pierce, "Application of ree-eyring generalized flow theory to suspensions of spherical particles," *Journal of colloid science*, vol. 11, no. 1, pp. 80–95, 1956.

[25] F. A. Dullien, *Porous media: fluid transport and pore structure*. Academic press, 2012.

[26] D. Geldart, "Types of gas fluidization," *Powder technology*, vol. 7, no. 5, pp. 285–292, 1973.

[27] R. A. Brekken, "Gas fluidization of wheat flour in a stirred bed," 1968.

[28] M. Özbey and M. Söylemez, "Effect of swirling flow on fluidized bed drying of wheat grains," *Energy conversion and management*, vol. 46, no. 9, pp. 1495–1512, 2005.

[29] M. F. Mohideen, S. M. Seri, and V. R. Raghavan, "Fluidization of geldart type-d particles in a swirling fluidized bed," in *Applied Mechanics and Materials*, vol. 110. Trans Tech Publ, 2012, pp. 3720–3727.

[30] J. Howard, *Fluidized bed technology: principles and applications*. Adam Hilger, 1989.

[31] W. Vlasblom, *Designing Dredging Equipment*, 2003.

[32] D. Wilmoth, "Jet agitation dredging system," Oct. 26 1999, uS Patent 5,970,635. [Online]. Available: https://www.google.nl/patents/US5970635

[33] S. Vandycke, "Method and device for dredging underwater ground layers," Sep. 17 2002, uS Patent 6,449,883. [Online]. Available: https://www.google.nl/patents/US6449883

[34] A. Briggs and R. Nathenson, "Apparatus for excavating soil and the like using supersonic jets," Jun. 26 1990, uS Patent 4,936,031. [Online]. Available: https://www.google.nl/patents/US4936031

[35] F. Masaichi, "Fluidized drying apparatus," Sep. 22 1970, uS Patent 3,529,359. [Online]. Available: https://www.google.nl/patents/US3529359

[36] T. E. Toolbox, "Dry air properties," https://www.engineeringtoolbox.com/dry-air-properties-d_973.html, last visited: 12-11-2017.

[37] *in line floating ball flow meter*, Kytola instruments, 7 2016.

[38] *Ultrasonic Ranging Module*, Elec Freaks.

[39] Airpress, "Compressor hl 425-50," https://airpress.nl/compressor-hl-425-50, last visited: 30-10-2017.

Appendix A: Raw Data
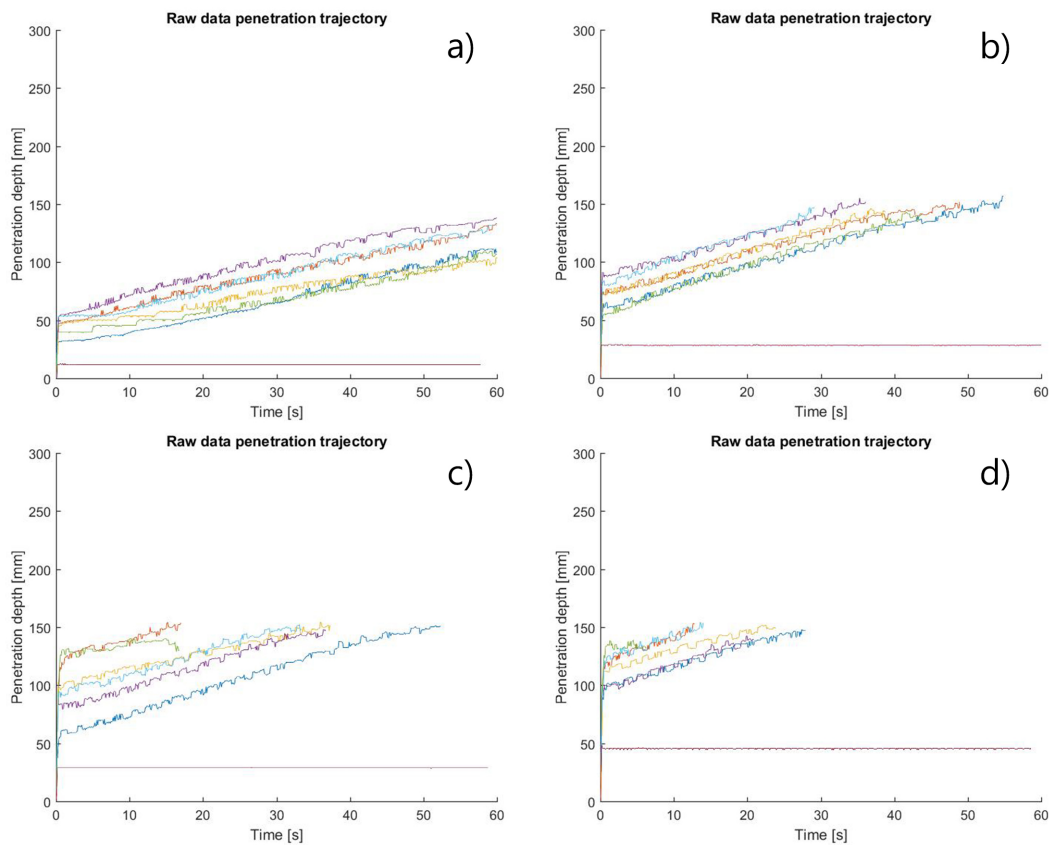
Figure A.1: Raw data of all repetitions for the mass variation using the glass beads of category A (40-70μm) and the reference data. Every colour shows the trajectory of a repetition. The red line shows the repetition without airflow and is called the reference. a) Repetitions with a penetration tool mass of 0.8 kg and an airflow of 25 l/min. b) Repetitions with a penetration tool mass of 1.3 kg and an airflow of 25 l/min. c) Repetitions with a penetration tool mass of 1.8 kg and an airflow of 25 l/min. d) Repetitions with a penetration tool mass of 2.3 kg and an airflow of 25 l/min.
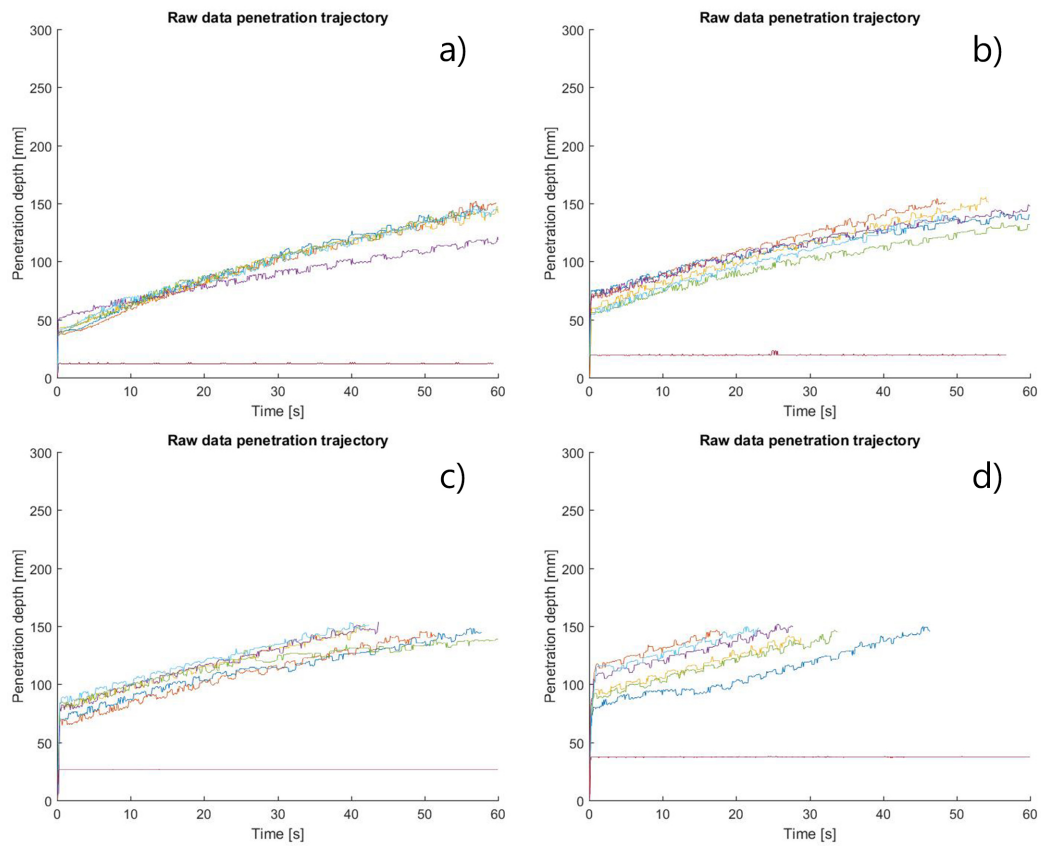
Figure A.2: Raw data of all repetitions for the mass variation using the glass beads of category B (150-250μm) and the reference data. Every colour shows the trajectory of a repetition. The red line shows the repetition without airflow and is called the reference. a) Repetitions with a penetration tool mass of 0.8 kg and an airflow of 25 l/min. b) Repetitions with a penetration tool mass of 1.3 kg and an airflow of 25 l/min. c) Repetitions with a penetration tool mass of 1.8 kg and an airflow of 25 l/min. d) Repetitions with a penetration tool mass of 2.3 kg and an airflow of 25 l/min.
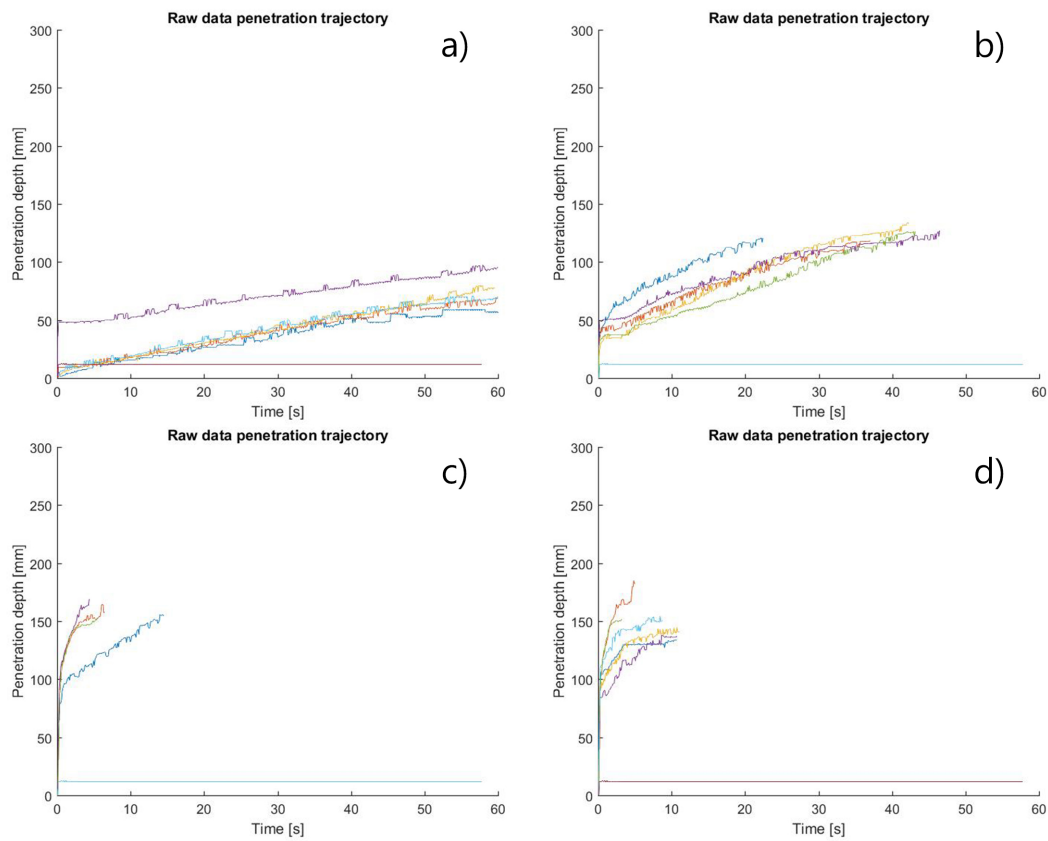
Figure A.3: Raw data of all repetitions for the airflow variation using the glass beads of category A (40-70µm) and the reference data. Every colour shows the trajectory of a repetition. The red line shows the repetition without airflow and is called the reference. a) Repetitions with a penetration tool mass of 0.8 kg and an airflow of 25 l/min. b) Repetitions with a penetration tool mass of 0.8 kg and an airflow of 50 l/min. c) Repetitions with a penetration tool mass of 0.8 kg and an airflow of 75 l/min. d) Repetitions with a penetration tool mass of 0.8 kg and an airflow of 100 l/min.
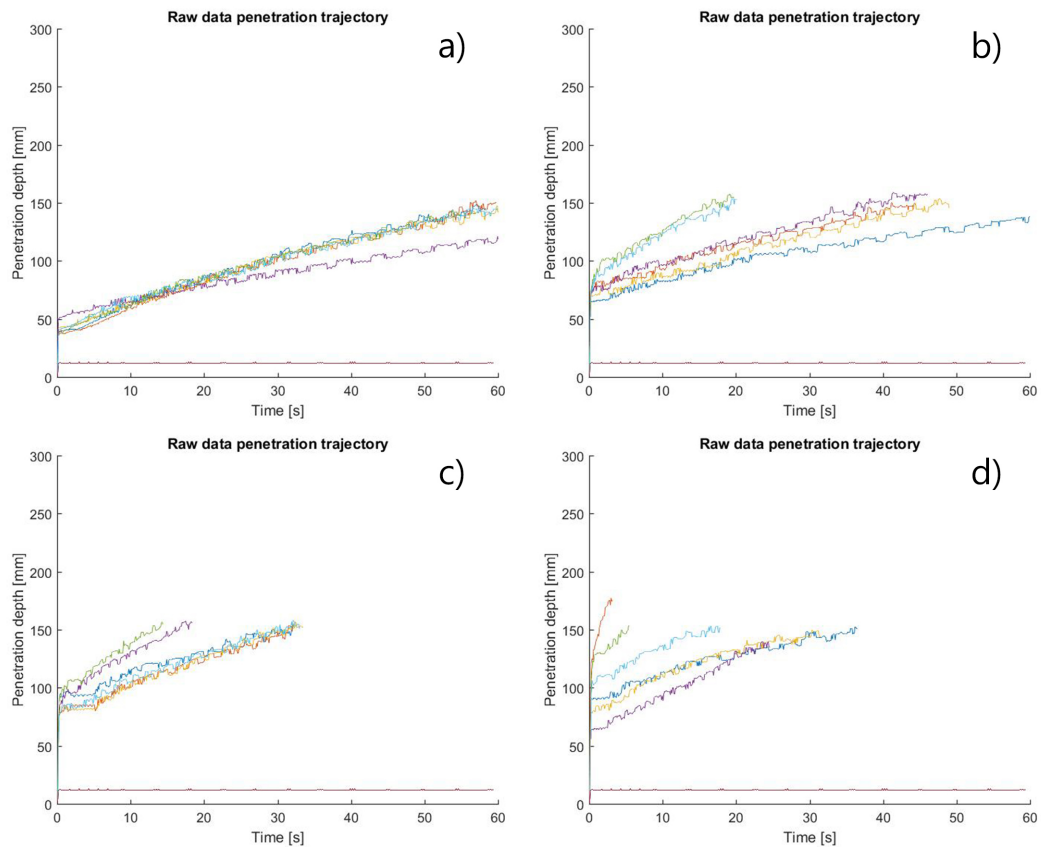
Figure A.4: Raw data of all repetitions for the airflow variation using the glass beads of category B (150-250μm) and the reference data. Every colour shows the trajectory of a repetition. The red line shows the repetition without airflow and is called the reference. a) Repetitions with a penetration tool mass of $0.8\ kg$ and an airflow of $25\ l/min$. b) Repetitions with a penetration tool mass of $0.8\ kg$ and an airflow of $50\ l/min$. c) Repetitions with a penetration tool mass of $0.8\ kg$ and an airflow of $75\ l/min$. d) Repetitions with a penetration tool mass of $0.8\ kg$ and an airflow of $100\ l/min$.
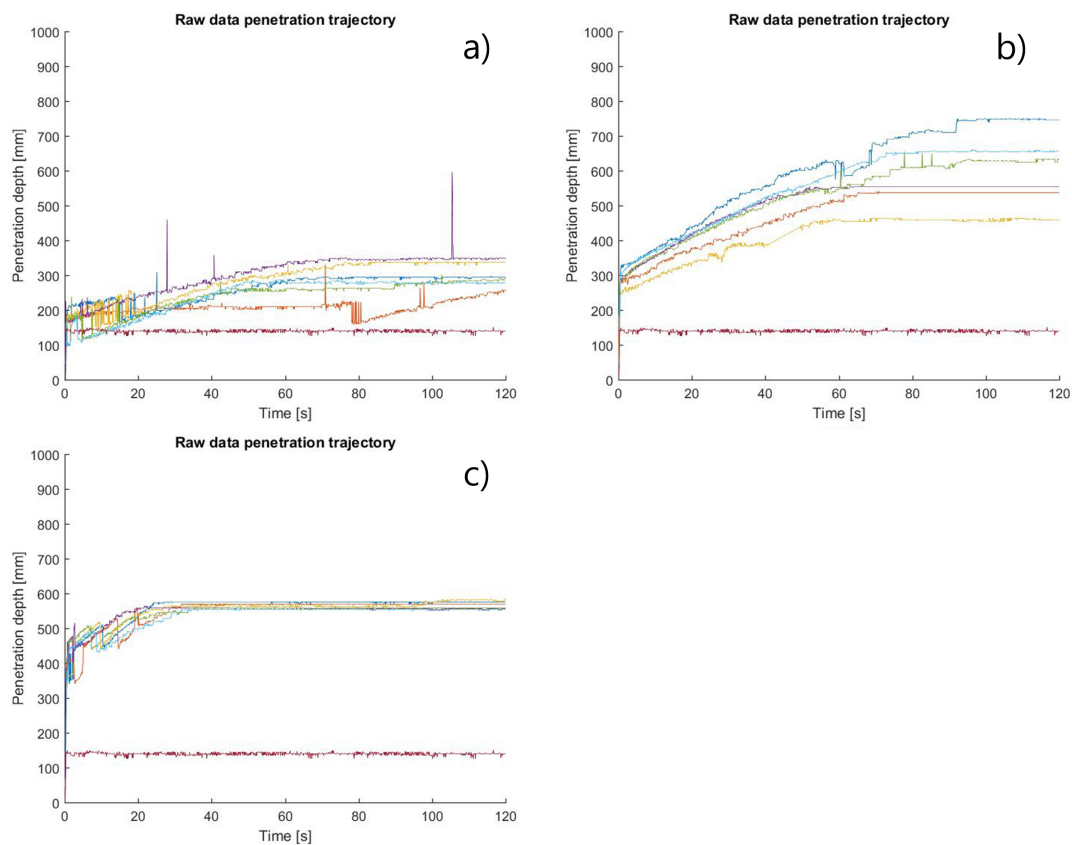
Figure A.5: Raw data of the deep experiment using the glass beads of category B (150-250µm) and the reference data.Every colour shows the trajectory of a repetition. The red line shows the repetition without airflow and is called the reference. a) Repetitions with a penetration tool mass of 5.5 kg and an airflow of 50 l/min. b) Repetitions with a penetration tool mass of 5.5 kg and an airflow of 100 l/min. c) Repetitions with a penetration tool mass of 5.5 kg and an airflow of 150 l/min.

B

Appendix B: Matlab

B.1. Main file experiment 1 and 2

```matlab
1  %%  Author: Michael Kunne
2  %%  Date: 29−8
3  %%  Description: Define dataset to be analysed. Perform basic statistics.
4  %%              Save outcome for later usage and make figures for the
5  %%              first comparison. Experiment 1 and 2
6  %%
7
8
9  %% start
10 clc
11 close all
12 clear all
13
14 %% Which data must be selected
15 Dataset = 'E' ; % See readme
16 [Height,Time] = RawData(Dataset); % Load in data
17 range = [1:6]; % Data range to be analysed
18
19
20 %% Load reference data
21 ref_Dataset = 'X'; %X for small, Z for Medium size, Y for deep experiment
22 [ref_Height,ref_Time] = RawData(ref_Dataset);
23 ref = 1;           % Reference dataset, see readme
24
25 %% Plot raw data
26
27 figure
28 for h = range
29
30
31     Time(:,h) = Time(:,h) − Time(1,h);          % Start all data on t=0
32     plot(Time(:,h)/1000,Height(:,h))            % Plot position as a
           function of time of dataset
33     hold on
34
35     title('Trajectory')
36     xlabel('Time [s]')
37     ylabel('Height [mm]')
```

```matlab
38      axis([0 60 0 300])
39      ref_Time(:,ref) = ref_Time(:,ref) − ref_Time(1,ref);    % Start
            reference on t=0
40      plot(ref_Time(:,ref)/1000,ref_Height(:,ref))            % Plot
            reference data
41
42      %% Calculate propagation velocity
43      A = Height(:,h);
44      A(~any(~isnan(A), 2),:)=[];
45
46      x10 = Height(floor(length(A)*0.1),h);   % First point is at 10% of the
             data
47      t10 = Time(floor(length(A)*0.1),h);
48      x90 = Height(floor(length(A)*0.9),h);   % End point is at 90% of the
            data
49      t90 = Time(floor(length(A)*0.9),h);
50      dx = x10 − x90;                         % Calculate difference in
            height
51      dt = t90 − t10;                         % Calculate difference in time
52      v(h) = dx/dt;                           % Average velocity
53  end
54
55  %% Plot propagation veloxity velocity
56  if length(range)>6
57      v1 = nanmean(v(1:6));
58      v2 = nanmean(v(7:12));
59      v3 = nanmean(v(13:18));
60      v4 = nanmean(v(19:24));
61      V = [v1 v2 v3 v4];
62      Y = [0.8 1.3 1.8 2.3];  % Testconditions [25 50 75 100] for airflow,
            [0.8 1.3 1.8 2.3] for mass
63
64      % Calculate Maximum for errorbar
65      vmax1 = nanmax(v(1:6));
66      vmax2 = nanmax(v(7:12));
67      vmax3 = nanmax(v(13:18));
68      vmax4 = nanmax(v(19:24));
69      Vmax = [vmax1 vmax2 vmax3 vmax4];
70
71      % Calculate Minimum for errorbar
72      vmin1 = nanmin(v(1:6));
73      vmin2 = nanmin(v(7:12));
74      vmin3 = nanmin(v(13:18));
75      vmin4 = nanmin(v(19:24));
76      Vmin = [vmin1 vmin2 vmin3 vmin4];
77
78      % Plot errorbar figure
79      figure
80      errorbar(Y,V*1000,Vmin*1000,Vmax*1000)
81      title('Average propagation velocity')
82      xlabel('Tool mass [kg]')    % Variable Tool mass [kg] or Airflow [L/
            min]
83      ylabel('Velocity [mm/s]')
84      axis([0.5 2.5 0 10])
85      set(gca,'xtick',0.8:0.5:2.3)
86
```

```matlab
87      % Statistical analysis of propagation velocities
88      V_anova = [v(1:6);v(7:12);v(13:18);v(19:24)]';
89      [p,tbl,stats] = anova1(V_anova)
90      multcompare(stats)
91  end
92  %% Smooth data
93
94  figure
95  for h = range
96
97
98      plot(smooth((Time(:,h)/1000),15),smooth((Height(:,h)),15)) % Smooth
            data plot
99      hold on
100
101     title('Trajectory')
102     xlabel('Time [s]')
103     ylabel('Height [mm]')
104     axis([0 60 0 300])
105     ref_Time(10:end,ref) = ref_Time(10:end,ref) - ref_Time(1,ref);
106     plot(smooth((ref_Time(10:end,ref)/1000),9),smooth(ref_Height(10:end,
            ref),9))
107
108
109  end
110
111  %% Calculating average Height for range
112  for h = range    % Find the shortest vector. Make a average upto that point
113      length_Height(h-(range(1)-1)) = length(Height(~isnan(Height(:,h))));
114  end
115  min_Length = min(length_Height);
116
117  s60 = Height(1:min_Length,range); % Take the length of the shortest vector
          in the range, create an average, take data sample for the selected
        range
118  Avg  = mean(s60,2);                % Calculate the averages
119
120  % Plot average
121  figure
122  plot(Time(1:length(Avg),range(1))/1000,smooth(Avg,'rlowess'))
123      title('Average Trajectory')
124      xlabel('Time [s]')
125      ylabel('Height [mm]')
126      axis([0 60 0 300])
127      hold on
128  plot(Time(1,range(1))/1000,Avg(1),'*');
129  plot(smooth((ref_Time(:,ref)/1000),'rlowess'),smooth(ref_Height(:,ref),'
        rlowess'))
130
131  %% Rearange data from Height to Depth
132  [m,n] = size(Height);
133  figure
134  axis([0 60 0 300])
135  hold on
136  for i = range
137      depth(:,i) = -(Height(:,i)-Height(1,i));
```

```matlab
138        plot(Time(:,i)/1000,depth(:,i))
139  end
140  ref_depth = -(ref_Height(:,ref) - ref_Height(1,ref));
141  plot(ref_Time(:,ref)/1000,ref_depth)
142
143
144  %% Average depth
145  s60 = depth(1:min_Length,range); % take the length of the shortest vector
         in the range, create an average, take data sample for the selected
         range
146  Avg_dept  = mean(s60,2);
147
148  % Plot average depth
149  figure
150  plot(Time(1:length(Avg_dept),range(1))/1000,smooth(Avg_dept,'rlowess'))
151        title('Average Trajectory')
152        xlabel('Time [s]')
153        ylabel('Depth [mm]')
154        axis([0 60 0 300])
155        hold on
156  plot(Time(1,range(1))/1000,Avg_dept(1),'k*');
157  plot(smooth((ref_Time(:,ref)/1000),'rlowess'),smooth(ref_depth,'rlowess'),
         'r')
158  t_avg = Time(1:length(Avg_dept),range(1))/1000;
159  save(strcat(Dataset,mat2str(range),'avg'), 'Avg_dept','t_avg') % Save data
         for combined plots and statistics
160
161
162  %% Initial penetration depth
163  depth1=depth(10,range);                          % Initial penetration
         equals 10th datapoint
164  save(strcat(Dataset,mat2str(range)), 'depth1') % Save data for combined
         plots and statistics
```

B.2. Main file experiment 3

```matlab
%% Author: Michael Kunne
%% Date: 29−8
%% Description: Define dataset to be analysed. Perform basic statistics.
%%              Save outcome for later usage and make figures for the
%%              first comparison. Experiment 3
%%


%% start

clc
close all
clear all

%% Which data must be selected
Dataset = 'L' ; % See readme
[Height,Time] = RawData(Dataset);
range = [1:6]; % Data range to be analysed


%% Load reference data
ref_Dataset = 'Y'; %X for small, Z for Medium size, Y for depth experiment
[ref_Height,ref_Time] = RawData(ref_Dataset);
ref = 1;           % Reference dataset, see readme

%% Plot raw data
figure
for h = range


    Time(:,h) = Time(:,h) − Time(1,h);              % Start all data on t=0
    plot(Time(:,h)/1000,Height(:,h))                % Position as a function
        of time
    hold on

    title('Trajectory')
    xlabel('Time [s]')
    ylabel('Height [mm]')
    axis([0 120 0 1000])
    ref_Time(:,ref) = ref_Time(:,ref) − ref_Time(1,ref);   % Start
        reference on t=0
    plot(ref_Time(:,ref)/1000,ref_Height(:,ref))          % Plot
        reference data

end

%% smooth data

figure
for h = range

    plot(smooth((Time(:,h)/1000),15),smooth((Height(:,h)),15))
                    % Smooth data plot
```

```matlab
51        hold on
52
53        title('Trajectory')
54        xlabel('Time [s]')
55        ylabel('Height [mm]')
56        axis([0 120 0 1000])
57        ref_Time(10:end,ref) = ref_Time(10:end,ref) − ref_Time(1,ref);
58        plot(smooth((ref_Time(10:end,ref)/1000),9),smooth(ref_Height(10:end,
             ref),9))
59
60
61  end
62
63  %% Calculating average Height for range
64  for h = range    % Find the shortest vector. Only make a average upto that
         point
65        length_Height(h−(range(1)−1)) = length(Height(~isnan(Height(:,h))));
66  end
67  min_Length = min(length_Height);
68
69  s60 = Height(1:min_Length,range); % Take the length of the shortest vector
          in the range, create an average, take data sample for the selected
         range
70  Avg  = mean(s60,2);                    % Calculate the averages
71  figure
72  plot(Time(1:length(Avg),range(1))/1000,smooth(Avg,'rlowess'))
73        title('Average Trajectory')
74        xlabel('Time [s]')
75        ylabel('Height [mm]')
76        axis([0 120 0 1000])
77        hold on
78  plot(Time(1,range(1))/1000,Avg(1),'*');
79  plot(smooth((ref_Time(:,ref)/1000),'rlowess'),smooth(ref_Height(:,ref),'
         rlowess'))
80
81  %% Rearange data from Height to Depth
82  [m,n] = size(Height);
83  figure
84  axis([0 120 0 1000])
85  hold on
86  for i = range
87        depth(:,i) = −(Height(:,i)−Height(1,i));
88        plot(Time(:,i)/1000,depth(:,i))
89  end
90  ref_depth = −(ref_Height(:,ref) − ref_Height(1,ref));
91  plot(ref_Time(:,ref)/1000,ref_depth)
92
93
94  %% Average depth
95  s60 = depth(1:min_Length,range); % take the length of the shortest vector
          in the range, create an average, take data sample for the selected
         range
96  Avg_dept  = mean(s60,2);
97
98  % Plot average depth
99  figure
```

```matlab
100  plot(Time(1:length(Avg_dept),range(1))/1000,smooth(Avg_dept,'rlowess'))
101      title('Average Trajectory')
102      xlabel('Time [s]')
103      ylabel('Depth [mm]')
104      axis([0 120 0 1000])
105      hold on
106  plot(Time(1,range(1))/1000,Avg_dept(1),'k*');
107  plot(smooth((ref_Time(:,ref)/1000),'rlowess'),smooth(ref_depth,'rlowess'),
         'r')
108  t_avg = Time(1:length(Avg_dept),range(1))/1000;
109  save(strcat(Dataset,mat2str(range),'avg'), 'Avg_dept','t_avg') % Save data
         for combined plots and statistics
110
111  %% Initial penetration depth
112  depth1=depth(10,range);                        % Initial penetration
         equals 10th datapoint
113  save(strcat(Dataset,mat2str(range)), 'depth1') % Save data for combined
         plots and statistics
114
115  % Plot initial penetration depth
116  figure
117  boxplot(depth1)
```

B.3. Load raw data

```matlab
%% Author: Michael Kunne
%% Date: 29-10
%% Description: Create filenames and load the .csv files with those names.
%%

function [Height, Time] = RawData(X)

% Initiate matrices
Height = zeros(2000,30);
Time = zeros(2000,30);

    for k = 1:30
        % Create a text file name, and read the file.
        filename = [X num2str(k) '.csv'];
        if exist(filename, 'file')
            [a,b] = importfile(filename);
            Height(1:length(a),k) = a;
            Time(1:length(a),k) = b;
        else
            fprintf('File %s does not exist.\n', filename);
        end
    end
% Remove zeros from data
  Height(Height==0) = NaN;
  Time(Time==0) = NaN;

% remove empty rows
  Height(~any(~isnan(Height),2),:)=[];
  Time(~any(~isnan(Time),2),:)=[];
  Height(:,~any(~isnan(Height)))=[];
  Time(:,~any(~isnan(Time)))=[];
```

B.4. Plot average data of multiple experiments

```matlab
%% Author: Michael Kunne
%% Date: 29-8
%% Description: Load average data matrices and plot them together
%%

clc
clear all
close all

%% Data of H, mass variation big grain size, 25l/min
AVG_1 = load('H[1 2 3 4 5 6]avg.mat');
AVG_2 = load('H[7 8 9 10 11 12]avg.mat');
AVG_3 = load('H[13 14 15 16 17 18]avg.mat');
AVG_4 = load('H[19 20 21 22 23 24]avg.mat');

figure
hold on
plot(AVG_1.t_avg, AVG_1.Avg_dept)
plot(AVG_2.t_avg, AVG_2.Avg_dept)
plot(AVG_3.t_avg, AVG_3.Avg_dept)
plot(AVG_4.t_avg, AVG_4.Avg_dept)

legend('0.8 kg','1.3 kg','1.8 kg','2.3 kg','Location','SouthEast')
title('Average trajectory as function of tool mass')
xlabel('Time [s]')
ylabel('Depth [mm]')
axis([0 60 0 150])

%% Data of G, mass variation small grain size, 25l/min
AVG_1 = load('G[1 2 3 4 5 6]avg.mat');
AVG_2 = load('G[7 8 9 10 11 12]avg.mat');
AVG_3 = load('G[13 14 15 16 17 18]avg.mat');
AVG_4 = load('G[19 20 21 22 23 24]avg.mat');

figure
hold on
plot(AVG_1.t_avg, AVG_1.Avg_dept)
plot(AVG_2.t_avg, AVG_2.Avg_dept)
plot(AVG_3.t_avg, AVG_3.Avg_dept)
plot(AVG_4.t_avg, AVG_4.Avg_dept)

legend('0.8 kg','1.3 kg','1.8 kg','2.3 kg','Location','SouthEast')
title('Average trajectory as function of tool mass')
xlabel('Time [s]')
ylabel('Depth [mm]')
axis([0 60 0 150])

%% Data of E, airflow variation small grain size, 0.8kg
AVG_1 = load('E[1 2 3 4 5 6]avg.mat');
AVG_2 = load('E[7 8 9 10 11]avg.mat');
AVG_3 = load('E[12 13 14 15 16]avg.mat');
AVG_4 = load('E[17 18 19 20 21 22]avg.mat');

figure
```

```matlab
55  hold on
56  plot(AVG_1.t_avg, AVG_1.Avg_dept)
57  plot(AVG_2.t_avg, AVG_2.Avg_dept)
58  plot(AVG_3.t_avg, AVG_3.Avg_dept)
59  plot(AVG_4.t_avg, AVG_4.Avg_dept)
60
61  legend('25 l/min','50 l/min','75 l/min','100 l/min','Location','SouthEast'
        )
62  title('Average trajectory as function of airflow')
63  xlabel('Time [s]')
64  ylabel('Depth [mm]')
65  axis([0 60 0 150])
66
67  %% Data of I, airflow variation big grain size, 0.8kg
68  AVG_1 = load('I[1 2 3 4 5 6]avg.mat');
69  AVG_2 = load('I[7 8 9 10 11 12]avg.mat');
70  AVG_3 = load('I[13 14 15 16 17 18]avg.mat');
71  AVG_4 = load('I[19 20 21 22 23 24]avg.mat');
72
73  figure
74  hold on
75  plot(AVG_1.t_avg, AVG_1.Avg_dept)
76  plot(AVG_2.t_avg, AVG_2.Avg_dept)
77  plot(AVG_3.t_avg, AVG_3.Avg_dept)
78  plot(AVG_4.t_avg, AVG_4.Avg_dept)
79
80  legend('25 l/min','50 l/min','75 l/min','100 l/min','Location','SouthEast'
        )
81  title('Average trajectory as function of airflow')
82  xlabel('Time [s]')
83  ylabel('Depth [mm]')
84  axis([0 60 0 150])
```

B.5. Box plot and statistics of initial penetration

```matlab
%% Author: Michael Kunne
%% Date: 29-10
%% Description: Load data saved with the main script. Make a boxplot of
%%              initial penetration. Perform basic statistical analysis
%%

clc
clear all
close all

%% Load data

D1 = load('I[1 2 3 4 5 6].mat');
D2 = load('I[7 8 9 10 11 12].mat');
D3 = load('I[13 14 15 16 17 18].mat');
D4 = load('I[19 20 21 22 23 24].mat');

%% define experimental conditions for X label
m = [25 50 75 100];

%% create boxplot
D = [D1.depth1; D2.depth1; D3.depth1; D4.depth1]';
boxplot(D,m)
axis([0.5 4.5 0 150])
title('Effect of airflow on initial penetration depth (mass 0.8 kg)')
xlabel('Airflow [l/min]')
ylabel('Penetration depth [mm]')

%% statistics
[p,tbl,stats] = anova1(D)
multcompare(stats)
```

C

Appendix C: Arduino

```arduino
1  // defines pins numbers
2  const int trigPin = 9;
3  const int echoPin = 10;
4
5  // defines variables
6  float duration;
7  float distance;
8  void setup() {
9
10 pinMode(trigPin, OUTPUT); // Sets the trigPin as an Output
11 pinMode(echoPin, INPUT); // Sets the echoPin as an Input
12 Serial.begin(9600); // Starts the serial communication
13 }
14 void loop() {
15
16 // Clears the trigPin
17 delay(98);
18 delayMicroseconds(8);
19 digitalWrite(trigPin, LOW);
20 delayMicroseconds(2);
21
22 // Sets the trigPin on HIGH state for 10 micro seconds
23 digitalWrite(trigPin, HIGH);
24 delayMicroseconds(10);
25 digitalWrite(trigPin, LOW);
26
27 // Reads the echoPin, returns the sound wave travel time in microseconds
28 duration = pulseIn(echoPin, HIGH);
29
30 // Calculating the distance
31 distance= duration*0.34/2;
32
33 // Prints the distance on the Serial Monitor
34 Serial.print(String(distance,2));
35 Serial.print(";");
36 Serial.println(millis());
37 }
```

Appendix D: Averaging Example
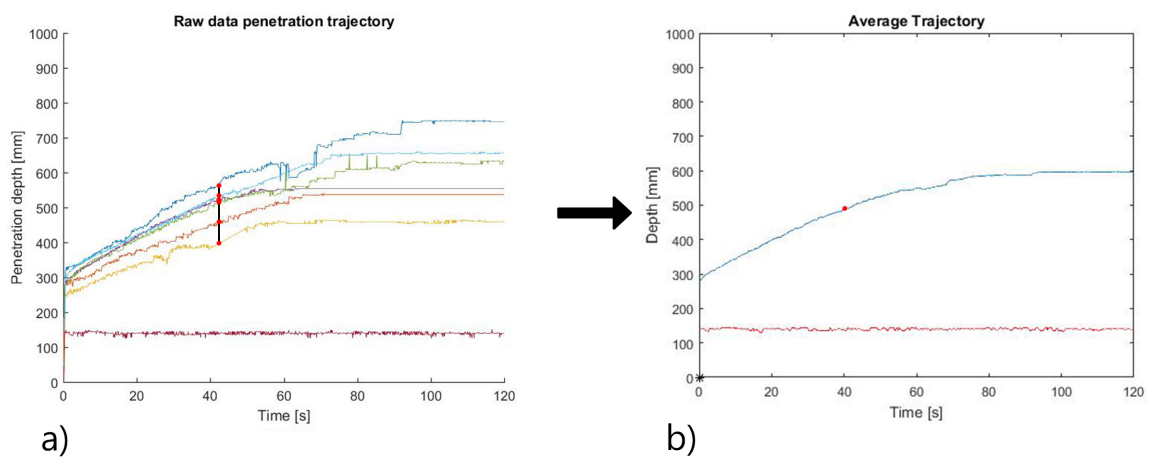
Figure D.1: Example computation of the average trajectory. The average is computed as the average depth on a point in time. a) Shows the raw data with the six depths on 40 s denoted with red dots. b) Shows the resulting average trajectory with the red dot showing the result of the averaging at 40 s